AD NUMBER

AD881923

LIMITATION CHANGES

TO:

Approved for public release; distribution is unlimited.

FROM:

Distribution authorized to U.S. Gov't. agencies and their contractors; Critical Technology; 18 NOV 1970. Other requests shall be referred to Air Force Technical Applications Center, Attn: VSC, Alexandria, VA 22313. This document contains export-controlled technical data.

AUTHORITY

AFTAC ltr, 1 May 1972

AN AUTOMATIC EVENT DETECTOR AT TFO

18 November 1970

Prepared For
AIR FORCE TECHNICAL APPLICATIONS CENTER
Washington, D. C.

By
R. R. Blandford
SEISMIC DATA LABORATORY

Under

Project VELA UNIFORM

Sponsored By
ADVANCED RESEARCH PROJECTS AGENCY
Nuclear Monitoring Research Office
ARPA Order No. 624

AN AUTOMATIC EVENT DETECTOR AT TFO

SEISMIC DATA LABORATORY REPORT No. 263

AFTAC Project No.:	VELA T/0706
Project Title:	Seismic Data Laboratory
ARPA Order No.:	624
ARPA Program Code No.:	9F10
Name of Contractor:	TELEDYNE GEOTECH
Contract No.:	F33657-70-C-0941
Date of Contract:	01 April 1970
Amount of Contract:	$ 1,785,000
Contract Expiration Date:	30 June 1971
Project Manager:	Royal A. Hartenberger (703) 836-7647

P. O. Box 334, Alexandria, Virginia

This document is subject to spe ial export controls and each transmittal to foreign governments or foreign nationals may be made only with prior approval of Chief, AFTAC. VSC
Alex, Va 22313

This research was supported by the Advanced Research Projects Agency, Nuclear Monitoring Research Office, under Project VELA-UNIFORM and accomplished under technical direction of the Air Force Technical Applications Center under Contract F33657-70-C-0941.

ABSTRACT

The on-line operation of a Fisher detector has been evaluated at the Tonto Forest Observatory short-period seismic array. Using 31 seismometers and one fixed threshold, the 90 percent incremental detection threshold on the Kuril Islands beam, centered at $\Delta = 70°$, is $m_b = 4.15 \pm .05$; with an experimentally determined false alarm rate of 0.17 per day. This compares favorably with the capabilities of a human operator. Storms in the Kurils significantly affect the distribution of amplitudes of the Fisher detection trace; and we estimate that most of the false alarms observed at the operating threshold can be traced to the statistical bias introduced by this storm-generated energy. If the threshold were adjusted to maintain a constant false alarm rate, the maximum effect on the threshold magnitude would be 0.05 m_b.

TABLE OF CONTENTS

LIST OF FIGURES

LIST OF FIGURES (Cont'd.)

LIST OF FIGURES (Cont'd.)

LIST OF FIGURES (Cont'd.)

INTRODUCTION

The purpose of this report is to describe the background and the present status of the Fisher detector of seismic signals and to compare its efficiency with other types of detectors.

Two basic types of automatic detectors of seismic signals have been investigated in the past. In the first, a short term average of the rectified or squared seismogram is compared to a longer term average; when the ratio exceeds a threshold, a detection is declared. In the second type, a checking procedure is either explicitly or implicitly programmed to see whether several independent seismometers give a detection within specified time windows. This checking procedure is analogous to the procedures of a human operator and can reject data spikes, local events, and off-beam events.

The detector implemented by IBM personnel at SAAC (1969) is an example of the first type of detector. A full LASA beam is rectified and the result is averaged over approximately 2 seconds. This is output to a long-term exponential smoothing algorithm in which the n^{th} short-term exponential average is equal to $(1-\alpha)$ times the $(n-1)^{st}$ value plus α times the current rectified average. The time constant is typically set at 60 seconds. A fixed value of the ratio of the short-term average to the exponential average is the threshold for declaring a detection.

The IBM detector can be triggered by off-beam and local events. It is protected from triggering on data spikes because the raw data is limited to a fixed equivalent ground motion (11 mμ) and when such a value is beamed and averaged it does not create excursions large enough to cause a detection.

An earlier detector, developed by Lincoln Lab personnel (1965), calculated a similar short and long-term average on the traces

of the center seismometers of the E and F ring subarrays of LASA. If a threshold crossing occurred on several of the eight channels within 20 seconds of one another, a detection was declared. This detector will adequately reject data spikes, but, of course triggers on all seismic events regardless of azimuth. By narrowing the arrival windows to suit certain move-out velocities, one would trigger detections only on arrivals from a fixed epicentral region. However, this refinement was not programmed by Lincoln Labs. The other disadvantage of this particular detector is that it makes no use of the improvement in signal to noise on the beam.

The Fisher detector was first suggested by Melton and Bailey (1957). The essence of this detector is that the power on the beam is divided by the power of the difference between the beam and the individual channel seismograms averaged over all channels. To express this mathematically, consider an infinite velocity signal, then let the individual traces be given by $S_i(t)$. In general the traces will be shifted to form a beam given by $\hat{S} = (1/N) \sum_i S_i$. The residual error on each channel is given by $S_i - \hat{S}$ where $\hat{S}$ has been appropriately shifted for non-infinite velocity beams. The expression for the Fisher detector on N channels is given by

$$F = \frac{\frac{1}{2}N \overline{\left(\frac{1}{N} \Sigma S_i\right)^2}}{\frac{1}{2(N-1)} \cdot \overline{\Sigma (S_i - \hat{S})^2}} = \frac{(N-1)}{N} \cdot \frac{\overline{(\Sigma S_i)^2}}{\overline{\Sigma (S_i - \hat{S})^2}} \qquad (1)$$

where the bar indicates that a function has been averaged over some time window, i.e.

$$\overline{S}_i = \frac{1}{P} \sum_{t=1}^{P} S_i(t)$$

The expression (1.1) can be transformed to

$$F = \frac{(N-1)}{N} \cdot \frac{\overline{(\Sigma S_i)^2}}{\overline{\Sigma S_i^2} - \frac{1}{N}\overline{(\Sigma S_i)^2}} \qquad (2)$$

which is usually simpler to compute. If the individual channels have non-zero means, a term must be added to the numerator and the result is

$$F = \frac{N-1}{N} \cdot \frac{\overline{(\Sigma S_i)^2} - \frac{1}{P}\left[(\overline{\Sigma S_i})^2\right]}{\overline{\Sigma S_i^2} - \frac{1}{N}\overline{(\Sigma S_i)^2}} \qquad (3)$$

When a signal arrives, the output of this detector increases for two reasons. First, the beam power in the numerator increases. Second, for high signal-to-noise ratios, the denominator nearly vanishes. Note that this will not happen unless the signal has the proper move-out; otherwise the shifted beam cannot cancel the individual seismometer trace so the denominator remains large. In this way the Fisher detector checks that the signal is recorded by several seismometers. For an off-beam signal both the numerator and denominator increase proportionally and there is no increase in the ratio.

As discussed in the next section, these useful qualitative properties are complemented by the fact that the ratio has a well studied statistical distribution. The ratio follows the central F distribution in the absence of signal, and the non-central F distribution in the presence of signal. Thus it is possible to predict from established theory the probability of detection and false alarm rate for any combination of bandwidth, signal detection window and number of seismometers.

Although Melton and Bailey (1957) first discussed the possibility of using the Fisher criterion as a detector, they did not apply it to seismic data. Booker (1965) was the next to study the Fisher detector. His work was implemented in a program on a CDC 1604. He showed that the Fisher detector had considerable promise, and that it was superior to a polarity coincidence detector proposed by Melton and Karr (1957). However, Booker had available only data from closely-spaced observatory seismometers. Noise recorded by these seismometers is correlated in the signal band, which is contrary to the hypotheses of the Fisher detector. Booker recognized this fact, and saw the effects in his results. He expressed the hope that it would be possible to allow for the correlated noise by finding and setting a higher threshold than would be predicted from theory, and that this threshold would be stable.

An auxiliary processor was built by Texas Instruments to implement the Fisher detector in real time, and an evaluation of it was performed on line at CPO by Edwards, Benno, and Creasey (1967). They found that no stable threshold could be set, and advocated that a modification be made to the processor to allow for an adaptive threshold. From our present vantage point we can see that correlated noise between the nineteen closely spaced CPO seismometers was the cause of this difficulty, and that the detector would have been stable if only the three most widely spaced seismometers with a spacing of 2.9 kilometers had been used. The closest spacing for the full array was 0.3 kilometers.

Shumway and Husted (1969) showed how to extend the results of Booker to colored spectra, and also showed how to compute the probability of detection given the signal-to-noise ratio.

In March of 1969 the TI auxiliary processor was installed on the 37-element TFO array which has a minimum spacing of 4 km. For the first time it was operating on data which was uncorrelated in

the signal band. The principal conclusion of this report is that at TFO the Fisher detector performs in agreement with theory, and is an excellent detector when installed at an array whose seismometers are spaced widely enough.

If two signals arrive at the same time, one of them must be regarded as noise and detection is more difficult. A useful extension of the Fisher detector would therefore be detection of two or more signals simultaneously present. Shumway and Dean (1968) have presented the theory required to produce minimum variance, undistorted estimates for each of a multiple set of signals imbedded in a collection of independent stationarily correlated noise series. For the case of Gaussian noise, Shumway (1970) has presented the asymptotic maximum likelihood detector for each of the multiple signals in terms of the classical F statistic. Work is presently underway to develop the probability of detection and false alarm statistics for two signals in a horizontal array: and to test the theory on real data. This detector could be used to detect explosions set off on purpose during a large earthquake, and to detect and estimate the long period waves from two events for discrimination purposes. Long period waves frequently overlap in time since they are of long duration. The estimators are not the same as the so-called multichannel filter which treats one of the signals as noise and estimates a noise correlation or spectral matrix to apply in the single-signal, weighted minimum variance, undistorted procedure. It has the advantage that a multichannel filter can only be applied to estimate the second event and then only if a substantial portion of the first event, substantially uncontaminated by the second event, is available to serve as the noise sample. The estimators developed by Kobayashi and Welsh (1969), called by them optimum fidelity estimators, are special cases of those developed by Shumway and Dean.

THEORY

The basic derivations of the Fisher detector can be found in the references cited in the Introduction. Here we shall briefly review the notation, and present some new theoretical results on the detection capability of arrays using the Fisher detector. This theory is perhaps of more than academic interest since the evaluation of the Fisher detector in the next section shows it to behave in good agreement with theory and to be an excellent detector which might well be implemented in real systems.

The basic hypotheses under which the Fisher detector theory is valid are:

1. Identical, deterministic signal on each channel.

2. Independent, identically distributed, stationarily autocorrelated, Gaussian noise series on each channel.

The detector is actually only sensitive to the assumptions of equal signal waveform and of uncorrelated noise between channels. Non-Gaussian noise is permissible to the degree that the central limit theorem guarantees that the output of a narrow band filter operating on any distribution tends to a Gaussian distribution. The noise need be stationary only over the time window surrounding the signal, which, in the present application is only three seconds. The equality of the noise autocorrelations in the detection band is needed in order that power in the residual noise will be the same on each channel so that the average residual noise power will follow on chi-squared distribution. If this assumption is violated the detector may not follow the predictions of theory, but a stable threshold can probably be set.

Under the assumption that no signal is present, the probability of the detection trace exceeding a given value of F, say F_o, is

expressed by

$$P\left\{F\left[N_1,\ N_2,\ 0\right] \geq F_o\right\}. \tag{4}$$

Equation (4) gives the probability that any value of F drawn from an F distribution with N_1 and N_2 degrees of freedom, and with a non-centrality parameter (a function of the signal to noise ratio) of zero, will exceed F_o. Now in reference to equations (2) and (4), N_1 is the number of degrees of freedom in the numerator, N_2 is the degrees of freedom for the denominator, and λ equal to 0 in this case, is the non-centrality parameter.

The symbol for the non-centrality parameter is chosen to be in agreement with that in Abramowitz and Stegun (1964). The relation between λ and the signal to noise ratio on the beam is given by $\lambda = 2BT(S/N)^2$. Shumway and Husted, and Scheffe (1959) define their non-centrality parameter as δ^2 and the relation between λ and δ^2 is $\lambda = \delta^2$.

The degrees of freedom for N_1 for the numerator may be calculated as follows: samples per second x (band width/folding frequency) x signal time window = 2 x band width x signal time window = 2BT. The degrees of freedom N_2 for the denominator is given by (N-1) times N_1, where N is the number of channels.

The false alarm rate in false alarms per day, with a threshold set at F_o and a signal time window of length τ seconds is given by

$$\text{False Alarms per day} = P\{F[N_1,\ N_2,\ 0] \geq F_o\} \times \frac{24 \times 60 \times 60}{\tau} = \frac{P}{\tau} \times 8.65 \times 10^4 . \tag{5}$$

This equation may underestimate the false alarms since it assumes that if neither of two adjacent windows of length τ give a false alarm, then neither will an intermediate window composed of one-half of each. However, considering that this estimate would be highly correlated with estimates in the other two windows, the increase in the false alarm rate would certainly be much less than a factor of two. To the false alarm rate (FAR) corresponding to F_o calculated from equation (5) there corresponds a probability of detection for a fixed signal-to-noise level. This probability is given by

$$P\left\{F\left[N_1, N_2, \lambda\,(S/N)\right] \geq F_o\right\}$$

where $\lambda(S/N)$ is given by $\lambda = 2BT(S/N)^2$

To calculate actual probability of detection-false alarm curves it is obviously necessary to calculate the central and non-central F distributions. Tables of these distributions exist, however; the smallest value of P generally tabulated is 0.01, and from (5) with a time window of 3.0 seconds, this would imply 255 false alarms per day. Thus we need to evaluate these distributions for ranges outside the customary tables. The methods for doing so are given in Appendix I.

Figure 1 shows the F value corresponding to a particular false alarm rate for a succession of numbers of seismometers in an array. For example, with 31 elements in the array, and a false alarm rate of 0.1 per day, the threshold value for F is 10.92, using the left-hand scale. This figure, and all following ones assume 2BT=3.0 degrees of freedom in the numerator (see first paragraph in Section 3) and 3(N-1) in the denominator i.e. $N_1 = 3$, $N_2 = (N-1)3$.

Figures 2 through 7 show the false alarm rate as a function of the probability of detection. Each figure is for a different size

array; and, on each figure, each curve is for a different signal-to-noise ratio on the beam. For example, Figure 7 is for 31 elements; and, with a signal-to-noise ratio of 3.0 on the beam, one has a 90 percent probability of detection with a false alarm rate of 0.22 per day. We may mention here that the signal-to-noise ratio is defined as the ratio of the square-root of the signal power divided by the square root of the noise power in the frequency band and time window under consideration. If we assume that the rms noise in the signal window is equal to the rms noise before the signal, and that the signal itself is typically a segment of a sine wave; then to translate the signal-to-noise values given in this report to values in terms of zero-peak signal divided by rms noise one would multiply by 1.414. To the extent that the signal cannot be regarded as a sine wave in the 3-second window used in this report the multiplying factor would be greater to allow for the greater amplitude of one out of the three cycles. It is generally agreed (e.g. Clark, 1968) that the conversion between peak-to-peak/2 rms signal-to-noise values and peak-to-peak signal/maximum peak-to-peak noise is performed by dividing the former values by 3.0. Thus, to convert signal-to-noise ratios used in this report to those measured by the ratio of peak-to-peak values of signal and noise one would multiply by 1.414/3.0 equal to $0.47 \approx 0.5$.

Figure 8 shows the signal-to-noise ratio required at the seismometer level for 90 percent probability of detection as a function of the number of instruments in the array. There are four curves for four different false alarm rates. We see for example that for 31 instruments and for a false alarm rate of 0.1 per day, that the signal-to-noise ratio at the seismometer level must be 0.51. Also in Figure 8 is an indication of the range in magnitude and dB corresponding to a range in signal-to-noise ratios. We note that for all arrays with more than 20 elements that an increase in false

alarm rate of a factor of 1,000 yields a decreases in the magnitude detected of only 0.13.

The signal-to-noise required for a fixed probability of detection as a function of the number of seismometers is proportional to $N^{-1/2}$ for N greater than 20. Although there is probably a simple explanation for this fact, we have not found it as yet. It is clear from the figure that the signal-to-noise ratio required decreases much more rapidly than $N^{-1/2}$ for small values of N. This reflects the decreasing degrees of freedom in the denominator of the F statistic. A power detector, for which the noise estimate is determined by a long window on the beam in front of the signal, would not depart from $N^{1/2}$ in this way and therefore may have advantages for small arrays.

PROCEDURES

Figure 9 shows the MCF-Fisher prefilter used at TFO. It is a 23-point symmetric filter designed using program FILPLOT2, with the parameters as indicated on the figure. It is interesting that to force a null at 0.2 Hz to cancel the microseisms, the parameter which was adjusted was the number of points in the filter. For a time window of 3 seconds, the number of degrees of freedom allowed by this filter is 3.6, assuming a white signal spectrum in the pass-band. In our calculations we have rounded 3.6 to 3.0 because the algorithms for calculating the F distribution do not accept non-integral values of N_1 or N_2 and because the signal and noise spectra are not truly white.

It is important to determine properly the length of the signal time window. Intuition suggests that the window should be equal in length to the visible portion of the P-wave. Booker (1965) reported that he found this to be true. Edwards et al (1967) reported that the typical small signal was 3 seconds in duration; and that the detector seemed unstable when a window of only 2 seconds was used. In the present study we used a time window of 3 seconds. Booker also presented results to show that a sampling rate of 10 sps was adequate, however at TFO the processor operates at 20 sps. Thus the "time window" for the auxiliary processor was set to be 60 points.

A full presentation of the MCF and auxiliary processor control data for one set of MCF beams, including a Fisher detector on a Kuril beam is given in Appendix II, together with a history of the Fisher beams recorded on film and tape up to the present time, so that the interested researcher can use the data easily.

Figure 10 shows a map of the 37 element TFO array used. Elements 3, 5, 7, 8, 12, and 16 are not in the beam used by the Fisher detector, leaving a total array of only 31 elements.

The output of the Fisher detector is recorded both on magnetic tape in digital form, and on develocorder film. In measuring amplitudes from the develocorder it is important to follow systematic procedures because even an error of 0.1 cm, as seen on the film viewer, is significant. Since the film can slip up and down in the viewer, and since different viewers can yield slightly different measurements for the same point, it is essential always to use the same viewer, to allow the film to move only in one direction through the viewer, and to make all measurements along the vertical center line of the viewer.

Calibrations on the film were maintained by finding the lowest value of the Fisher in a 30 minute period, three times a day; 2-2:30, 12-12:30, and 22-22:30. Examination of the digital tape shows that the Fisher goes to zero at least every 10 minutes, and so these minimum values should be at the same place on the viewing screen if the calibration is to be held from beginning to end of the film. Readings are not accepted unless the minima are within 0.1 cm of one another. Conversion of the Fisher readings (in centimeters) are converted to F values by creating a full scale output from the Fisher detector which is registered on the film, and on the magnetic tape. Calibrations performed on 30 June and 3 August 1970 were within 0.1 cm of one another on the film and within four counts out of 715 on the digital tape. The Fisher output which is digital, is converted to analog form, transmitted to the Astrodata equipment, redigitized and recorded.

An unfortunate feature of the Fisher detector as implemented is that overflows occur for large events, either on or off beam. This is manifested on the develocorder film by a discontinuity in the Fisher trace. The same feature was noted by Edwards et al (1967); they state: "The MCF Auxiliary Processor system is limited to a 12-bit (66 db) dynamic range on input... Large signals of interest were clipped on input or during intermediate computations..."

Figure 11 shows the detector response at 0732 April 25, 1970. Traces 0-3 are beamed for a Δ of 30°, and azimuths of 0, 90, 180, and 270 degrees. Traces 4-7 are for a Δ of 100° and the same four azimuths. Trace 8 is for infinite velocity and trace 9 is aimed at the Kuril Islands, a Δ of 70° and an azimuth of 315°. All of these beams are filtered with the same 23 point filter shown in Figure 9. Trace 10 is the Kuril beam through a broader filter. Trace 11 is the Fisher detector itself, and trace 12 is the infinite velocity beam of the crossed array at TFO. We note that the signal is clearly detectable on traces 9 and 10, and that the detection trace rises smoothly to a large value. Figure 12 shows the arrival of another well-recorded event at 0111 on 9 April 1970. Data spikes are responsible for the patterns of "arrivals" to the left and right of the true arrival. Note that the detector is unaffected. Figure 13 shows the behavior of the detector on a weak event; and Figure 14 shows how it breaks down due to hardware over-flows for a large event on beam. Figure 15 shows the behavior of the detector during a large arrival on another beam. We note that the trace flattens out, suggesting, as is true, that it would be more difficult to detect an on-beam signal during this time interval. We note also the small sawtooth-like pattern on the Fisher trace indicating over-flow conditions during the largest arrivals.

RESULTS

Figure 16 shows the 3 dB contour of the TFO short period Kuril beam. Events used were those reported during the periods 8-30 April and 1-15 June 1970, from the region bounded by 20N-70N and 110E-160W. The arrival time of each event at the TFO center element was predicted, and the maximum value of the Fisher in a 20-second window centered at this time was recorded. Assuming a threshold at F = 10.3 and assuming that all breakdown points would have gone over this threshold if there had been no overflow, one may generate Figure 17 which gives the probability of detection as a function of magnitude. This figure suggests that the incremental 90 percent detection threshold magnitude is 4.15 ± .05.

An F value of 10.3, by Figure 1, for N = 31, corresponds to a theoretical false alarm rate of 0.2 per day. The develocorder records for 13 days selected at random between 08 April and 15 June were scanned for all excursions of the Fisher trace greater than F = 10.3. For 10 of the days there were no false alarms, and there was one each for three other days for a false alarm rate of 0.23 per day. The expected number of detections that are true events not reported can be calculated as approximately .06 per day. There were seven excursions over F = 10.3 during the 13 days which were traced to true events in either the Philippines or Southern Alaska; outside of the 3 dB contour.

Thus, in summary, there was an average of 2.0 true detections per day with a 90 percent threshold magnitude of 4.15 $\pm$ .05, 0.23 apparent false alarms per day, and 0.54 off-beam detections per day. Of the apparent false alarms, .06 might be unreported events, leaving an estimated true false alarm rate of 0.17.

Figure 18 shows the signal-to-noise value on the Kuril beam as a function of the Fisher value for all events with Fisher values greater than 10.3, and a few day's data for smaller values. The signal-to-noise value was determined from film measurements as the ratio of the peak-to-peak signal amplitude to the peak-to-peak noise amplitude in the previous 60 seconds. The discussion in the Theory section shows that we should multiply these signal-to-noise values by a factor close to 2.0 to convert them to the signal-to-noise values used elsewhere in this study. This would imply that the 10.3 threshold corresponds approximately to a signal-to-noise rms power ratio of 4.0 on the beam. Examination of Figure 7 shows that for 31 elements a false alarm rate on the order of 0.2, corresponding to a Fisher threshold of 10.3, with 90 percent probability of detection, does indeed require a rms signal-to-noise value of approximately 3.0. Thus we see that the detector behaves as predicted from theory when examined from this alternate direction.

Figure 19 is a plot of the probability that the Fisher trace exceeds a certain F value, as a function of F. The two solid curves are theoretical for non-centrality parameters of $\lambda = 0$ and 1.0. Also on the curve are experimentally determined points, each from two hours of data computed using program FISHDET2 from F values recorded on digital tape at TFO. We see that the histograms from successive two-hour periods of data are quite close together, showing that the detector statistics are stable. However, over longer periods of time, the statistics can be quite different. These differences are significant as can be seen by the vertical error bars giving

the 99 percent Kolmogorov-Smirnov confidence interval. If any two of these histograms are drawn from the same population, then the distance between them at every value of F will be less than this interval 99 percent of the time.

We observed that large probabilities correlate with storms in the Kurils region. Texas Instruments (1967) have also found storms to be a source of P-wave noise. Figure 20 presents the probability that $F \geq 2.0$ for the period 16-24 August 1970. United States Weather Bureau maps revealed that a low pressure system moved across the beam during this interval, and that its winds were at a maximum on the 19th. Figure 21 shows the correlation between the average of the six highest velocity readings inside the 3 db contour as reported on the Weather Bureau maps for the same time period, and the probability that $F \geq 2.0$. The solid dots are for the period 16-24 August, and the other points are as noted. Although there is considerable scatter, the trend is definite. Figures 22a, b, and c show the Weather Bureau maps for the points marked by a letter in Figure 19.

The theoretical value for P(F) at $F = 2.0$, $\lambda = 0$ is $P = 0.1$. The fact that for some days $P < 0.1$ cannot be explained by a non-centrality parameter different from 0.0. It is our present belief that values less than 0.1 arise on days when significant storm energy arrives at TFO from locations other than Kurils. We feel that this biases the data so that it is more difficult for an accidental fluctuation to look like a signal from the Kurils, leading to a low probability for high Fisher values. An illustration of this for a large off-beam signal was seen in Figure 15. The low points in Figure 20 correspond to days when the low-pressure system had moved out of the beam.

Leaving aside these times when there is an unknown lower false alarm rate (and some correspondingly lower probability of detection), the range in false alarms per day implied by non-centrality parameters ranging from 0.0 to that corresponding to the largest observed

probability value displayed in Figure 20, approximately $\lambda = 1.0$, is 0.2 to 1.90 false alarms per day. If one adjusted the threshold value of F to maintain a constant false alarm rate of 0.2 per day, the range of F values would lie between 10.3 and 12.7; and the corresponding range in signal-to-noise at the seismometer level would be 0.51 to 0.57; a range of 0.05 magnitude units. Thus, by adaptively adjusting the threshold one might hope to detect events 0.05 smaller on days for which there were no storms than on days when storms were present. The problem of how to predict the false alarm rate and probability of detection in the presence of weak signals from directions other than the target area is presently under investigation at SDL by means of simulation.

Figure 23 shows the threshold F value as a function of the resulting false alarm rate for a series of non-centrality parameters.

On Figure 16 some 3.9 magnitude events are plotted. Those with F values greater than 7.0 are plotted as solid circles. There is some tendency for greater detection closer to TFO, in agreement with the fact that the amplitude falls off slightly, somewhat less than 0.1 magnitude units on average, with distance in the range 45-85°. However, the result is not clearcut, as would be expected from known variances in the determination of magnitude.

In a study by Clark (1970), using the same 31 sensor TFO Kuril beam with a 0.7 to 2.5 Hz filter, an experienced analyst obtained a 90 percent detection threshold of $4.35 \pm .1$ m_b. Adequate records were not kept to enable an estimate of the false alarm rate, however the analyst (Paul DeFries) has estimated a rate comparable to that of the Fisher detector. Thus the Fisher detector is apparently comparable to or slightly better than an experienced analyst.

There is no available data on which to base a comparison with a power detector. However it is clear that the false alarm rate would have been much higher at TFO due to local and other off-beam events. There were also many events each day where relaxation pulses from the seismometers would have triggered a threshold detector; although limiting of the seismometer traces, as done in the IBM system, might have solved this problem.

DISCUSSION

The Fisher detector has been shown to give a 90 percent incremental threshold magnitude of 4.15 $\pm$ .05 when operating on a TFO 31-element Japan-Kurils beam. The corresponding true false alarm rate was found to be 0.17 per day. Questions which now arise are: will the detector work in agreement with theory when fewer elements, e.g. 7, 13, or 19, are used? How well will it work when the fewer elements are closely clustered yielding a much broader beam and thus more detections on-beam per day? What is the detection threshold for closer teleseismic distances? Can the detection threshold be lowered by widening the band-pass, especially toward the high-frequency end?

A study should also be made of the computing capacity required, with the latest available equipment, to implement the detector on a suite of world-covering beams in a realistic system for arrays of 7, 13, and 19 elements.

The Fisher detector should be monitored through the winter and hurricane seasons to see if there are a few days per year in which the detection threshold is lowered a more substantial amount by storms.

Work is now in progress at SDL to extend the detector so that it will work in the presence of another signal. It is our belief that this will prove to be the first "high-resolution" technique capable of "splitting" two simultaneous events to a degree superior to that of conventional beamforming.

Work is also in progress to determine the beam pattern of an array on which the Fisher detector is operating. This beam pattern will be expressed in terms of probability of detection; and of course the beam pattern will be different for different signal-to-noise ratios. Despite this complication the probability beam pattern

is the one truly relevant to the surveillance problem. It enables one to cover the earth with beams guaranteeing a particular probability of detection for some fixed magnitude.

Using the probability of detection false alarm curves deduced in this study, it will also be possible to deduce the corresponding curves for a network of stations.

ACKNOWLEDGEMENTS

The many contributions to this study by Robert Shumway are gratefully acknowledged. John Douglas performed the systems programming at TFO necessary to implement the detector, and Donald Reinbold did the film analysis at SDL.

REFERENCES

Abramowitz, M. and Stegun, I.A., 1964 Handbook of Mathematical Functions, Applied Mathematics Series No. 55, National Bureau of Standards.

Booker, A.H., 1965, Analysis of variance as a method for seismic signal detection, Seismic Data Laboratory Report No. 116, Teledyne Earth Sciences.

Clark, D., 1968, Preliminary beamforming study of the TFO-37 array, Seismic Data Laboratory Report No. 216, Teledyne Geotech.

Clark, D.M., 1970, LASA and TFO film analysis. Seismic Data Laboratory Memorandum, 27 January, Teledyne Geotech.

Edwards, J.P., Benno, S.A., and Creasey, G., 1967, Evaluation of the CPO Auxiliary Processor., CPO Special Report No. 5, Texas Instruments Science Services Division.

IBM Contract No. F19628-67-C-0198, final technical report, Experimental signal processing system, Volume I, 1969. (See also Kobayashi, H., and Welch, P.D., 1969, The detection and estimation of two simultaneous seismic events, in Proceedings of the Symposium on Computer Processing in Communication, Polytechnic Press, Brooklyn, New York.)

Melton, Ben S., and Bailey, Leslie F., 1957, Multiple signal correlators, Geophysics, v. 22, p. 565-588.

Melton, Ben S. and Karr, Leslie F., 1957, Polarity coincidence scheme for revealing signal coherence, Geophysics, v. 22.

Scheffe, H., 1959, The analysis of variance, Wiley.

Seismic Discrimination, 1965, Semiannual Technical Summary, 31 December 1965, Lincoln Labs, ESD-TDR-65-597.

REFERENCES (Cont'd.)

Shumway, R.H., 1970, Applied regression and analysis of variance for stationary time series, J. Am. Stat. Assn., v. 65, p. 332, in press.

Shumway, R.H., and Dean, W.C., 1968, Best linear unbiased estimation for multivariate stationary processes, Technometrics, v. 16, p. 523-534.

Shumway, R.H. and Husted, H.L., 1970, Frequency dependent estimation and detection for seismic arrays. Seismic Data Laboratory Report No. 242, Teledyne Geotech.

Texas Instruments Incorporated, 1967, Array research final report, Contract AF 33(657)-14648, 20 January.

APPENDIX I

CALCULATION OF THE F-DISTRIBUTION

Tables of the F distribution are available in Scheffé, (1959). However, they are tabulated only for values of P between 0.99 and 0.01. In addition they are printed in a form somewhat difficult to use. Equations for the F distribution are given by Abramowitz and Stegun, (1964). We used formulas 26.6.7 and 26.6.18. When we first attempted to use the formulas, the results did not agree with the tables in Scheffé. Ronald Finkler of Institute of Defense Analyses (personal communication) pointed out that for the equations to be correct, what appears as F' on the right hand side of equation 26.6.18 must be replaced by $F'\nu_1/(\nu_1 + 2j)$

Then the correct equations are:

26.6.6

$$Q(F|\nu_1, \nu_2) = x^{\frac{\nu_1+\nu_2-2}{2}} \left[1 + \frac{\nu_1+\nu_2-2}{2}\left(\frac{1-x}{x}\right) + \frac{(\nu_1+\nu_2-2)(\nu_1+\nu_2-4)}{2.4}\right.$$

$$\left(\frac{1-x}{x}\right)^2$$

$$\left. + \frac{(\nu_1+\nu_2-2)\cdots(\nu_2+2)}{2.4\cdots(\nu_1-2)}\left(\frac{1-x}{x}\right)^{\frac{\nu_1-2}{2}}\right] \quad \nu_1=N_1, \ \nu_2=N_2, \tag{1}$$

$$x = \frac{\nu_2}{\nu_2+\nu_1 F}, \ \nu_1 \text{ even}$$

$$Q = 1 - P$$

26.6.18

$$P(F'|\nu_1,\nu_2,\lambda) = \sum_{j=0}^{\infty} e^{-\lambda/2}\frac{(\lambda/2)^j}{j!} P\left(\frac{F'\nu_1}{\nu_1+2j}\middle|\nu_1+2j,\nu_2\right) \tag{2}$$

In the computer calculation use is made of the fact that successive terms in 26.6.7 may be calculated recursively. This formula is in the inner loop between statements 40 and 70.

```
      SUBROUTINE NCF(F,EL,N1,N2,U,J)
C RETURNS U, THE INTEGRAL FROM F TO INFINITY OF THE NON-CENTRAL F
C DISTRIBUTION WITH NON-CENTRALITY PARAMETER EL, AND N1 AND N2 DEGREES
C OF FREEDOM.  THE FORMULAS ARE 26.6.18 AND 26.6.7 IN AMS 55, HANDBOOK
C BUREAU OF STANDARDS EXCEPT THAT F-PRIME IN RHS OF 26.6.18 IS
C REPLACED BY (F*N1)/(N1+2J) AS IT MUST BE TO GET THE RIGHT ANSWER.
C ANSWER ACCURATE TO ABOUT ONE PART IN TEN TO THE SIXTH. IF NOT
C  ACHIEVED BY 2000 TERMS, AN ERROR MESSAGE RESULTS
C ALSO RETURNS J THE NUMBER OF TERMS TAKEN IN THE SERIES.
C N2 MUST BE EVEN
      EN1=N1 $ ELX=EXPF(-EL/2.) $ EL2=EL/2. $LJ=    EL2 + 1.1
      PS=.0 $ AJF=1. $ EL2J=1.
C  HERE ARE THE 2000 TERMS
      DO 10 J=1,2000
      AJ=J $ AJ1=J-1 $ U1=EN1 + 2.*AJ1 $ U2=N2 $ F1=(EN1/U1)*F
      X=U2/(U1*F1+U2) $ NUT=N2/2.-.9 $ U=U1+U2 $ XR=(1.-X)/X
      IF(NUT.EQ.0) 20,30
   30 T1=.5*(U-2.)/XR $ S=1.+T1 $ IF(NUT.GT.1) 40,60
   20 S=1. $GO TO 60
   40 DO 70 I=2,NUT
      EI=I $ T2=((.5/EI))*(U-2.*EI)/XR*T1 $ S=S+T2
   70 T1=T2
   60 E1=.5*(U-2.)$UC=((1.-X)**E1)*S$  PC=UC
      IF(EL.LT.1.E-10.AND.AJ1.LT.1.E-10) 80,90
   80 PS=PS+PC $ GO TO 101
   90 PA=PC*EL2J      $ PS=PS+PA $ IF(J.LT.L2)101,130
  130 T=(PA*ELX)/(1.-PS*ELX)
      IF(T.LT.1.E-07) 100,101
C TEST IS (DELTA U)/U LESS THAN 1.E-07 , SO LONG AS WE HAVE TAKEN
C ENOUGH TERMS TO GET THE MAXIMUM OF THE CONVERGING SERIES FOR
C EXPF(-L/2).
  101 CONTINUE
   10 EL2J=EL2J*EL2/AJ
  100 IF(J.GT.1999)110,120
  110 PRINT 1000 $ GO TO 120
 1000 FORMAT (10X,43H CONVERGENCE TEST FAILED TRY MORE TERMS-NCF)
  120 P=ELX*PS $ U=1.-P
      RETURN
      END
```

APPENDIX II

OPERATING SCHEDULES AND PARAMETERS

DATE	DATA GROUP FROM	TO	CHANNEL AND NAME FROM	TO	DISTANCE	AZIMUTH	FILTER CENTER FREQUENCY	FILTER NUMBER OF COEFFICIENTS	COMMENTS
06 February 70	7278	7291		9,BS7	70	315			
				12,MCF1	180	-			Kurils
				13,FSH	180	-			∞FSH
03 April 70									∞
				11,BS9	70	315	1.0	23	
				12,MCF1	70	315		19	Kurils
				13,FS4	70	315	1.0	23	Kurils
01 June 70									Kurils
			10,BS8	10,BS9	70	315	1.0	23	
			11,BS9	11,MCF1	70	315	1.4	31	Kurils
			12,MCF1	12,MCF2	70	315	1.6	27	Kurils
			13,FSH	13,FSH	70	315	1.0	23	Kurils
26 June 70									
				BS9			1.0	23	
				MCF1			1.4	31	Novaya Zemlya
				MCF2			1.6	27	Kurils
				Fisher			1.0	23	Kurils
01 July 70									Novaya Zemlya
			10,BS8	10,BS9	70	315	1.0	23	
			11,BS9	11,MCF1	70	315	1.4	31	Kurils
			12,MCF1	12,MCF2	70	315	1.6	27	Kurils
			13,FSH	13,FSH	70	315	1.0	23	Kurils
24 August 70									Kurils
			3,BS1	3,BS1	70	315	1.0	23	
			10,BS9	10,BS9	40	336	1.0	23	Kurils
			11,MCF1	11,MCF1	40	24	1.0	23	Aleutians
			12,MCF2	12,FSH	40	336	1.0	23	Hudson Bay
05 October 70									Aleutians
			10,BS9	10,BS9	40	24	1.0	23	
			11,MCF1	11,MCF1	40	336	1.0	23	Hudson Bay
			12,FS4	12,FSH	40	24	1.0	23	Aleutians
									Hudson Bay
21 October 70	7298	7299	11,MCF1	11,BS9	70	313	1.0	23	
			12,FSH	12,FSH	70	313	1.0	23	Kurils FTH Fisher Threshold
			13,WWV	13,FTH	70	313	1.0	23	Kurils 19-Element Beam
				14,WWV					Kurils

Changed to 7 elements January 20, 1971.

Changed to 31 elements March 1, 1971.

N2 040 from February 6 to August 3

006 from August 3 16:56 to September 4, 1970

040 September 4, 1700 to _____

Cal.#1 on 30 June 20:27 Tape No. 7857

Cal.#2 on 03 August 16:56 Tape No. 8079

Fisher Threshold set at 125_{10} from 0000 on 21 October 1970. Set to 134_{10} on October 28. Set to 160_{10} on November 23, 205_{10} on January 20, 125_{10} on March 1, 1971.

FSH History 000_{10} Data Truncator 1

N2 040_8 Summation Truncator 9

N1 777_8 Output Setting -15

MCF FORMAT

	Distance	Direction	Apparent Vel.
BS 0	30°	0°	12.33 km/sec
BS 1	30°	90°	12.33 km/sec
BS 2	30°	180°	12.33 km/sec
BS 3	30°	270°	12.33 km/sec
BS 4	100°	0°	24 km/sec
BS 5	100°	90°	24 km/sec
BS 6	100°	180°	24 km/sec
BS 7	100°	270°	24 km/sec
BS 8	180°	All	∞ Velocity
BS 9	70°	315°	18 km/sec

	Filter Points	Filter Characteristics
MCF 0	23 point filter	Beamed for 315°Az; 70° dist
MCF 1	19 point filter	Beamed for 315°Az; 70° dist
MCF 2	Not Used	
MCF 3	Not Used	
MCF 4	Not Used	
U.K.0	Not Used	
U.K.1	Not Used	
MCF P-1	Not Used	
MCF P-2	Not Used	
MCF P-3	Not Used	
MCF P-4	Not Used	
FISHER	Beamed for 315° Az; 70° dist.	

Operation Parameters for 3 April 1970
Date

Format Switch Settings to _____

3 0	0 8 0	1	9	0 8 0	0 5 3
Input Channels	Filter Points	MCF Outputs	BS Outputs	BS History	Timing Delay

GAIN: Input 0 db Output -0

MCF Ch.#	Input Cable #	B	BS0	BS1	BS2	BS3	BS4	BS5	BS6	BS7	BS8	BS9
0	100	1	46	46	46	46	46	46	46	46	46	46
1	101	2	50	36	32	44	45	37	35	43	41	46
2	102	4	52	63	54	43	52	57	54	47	53	46
3	103	6	41	41	53	53	43	44	51	50	46	46
4	104	9	56	43	24	37	50	42	32	40	41	46
5	105	10	62	57	30	33	53	52	37	40	45	46
6	106	11	57	71	47	35	55	62	51	44	53	46
7	107	13	47	73	71	45	54	66	64	52	60	46
8	108	14	40	63	76	53	47	61	67	55	57	46
9	109	15	36	52	72	56	45	53	63	55	54	46
10	110	17	35	25	47	57	37	33	45	51	42	46
11	111	18	40	15	32	55	37	25	33	45	35	46
12	112	19	45	21	23	47	41	25	27	42	34	46
13	113	20	55	16	1	40	43	22	13	34	27	46
14	114	21	60	32	6	34	46	32	20	34	33	46
15	115	22	64	47	14	31	52	44	26	34	40	46
16	116	23	66	63	22	25	55	54	33	34	44	46
17	117	24	64	73	36	27	57	62	43	40	51	46
18	118	25	63	105	53	31	61	72	55	44	57	46
19	119	26	57	113	67	33	61	77	65	47	63	46
20	120	27	51	107	77	41	57	76	71	52	64	46
21	121	28	44	102	106	50	54	74	76	56	65	46
22	122	29	37	76	113	54	51	72	101	60	65	46
23	123	30	34	62	106	60	46	62	74	60	61	46
24	124	31	30	46	102	64	42	51	64	73	55	46
25	125	32	25	31	73	67	36	40	62	60	50	46
26	126	33	30	21	56	65	35	32	51	54	43	46
27	127	34	32	11	42	63	34	23	40	51	36	46
28	128	35	34	00	24	60	32	14	26	44	30	46
29	129	36	42	5	16	53	37	16	23	42	30	46
30	130	37	50	13	10	45	40	21	20	37	30	46

Filter Points And Coefficients

MCF 0

Units

Tens	0	1	2	3	4	5	6	7	8	9
0	0000	0000	0000	0000	0000	0000	0000	0000	0000	0000
1	0000	0000	0000	0000	0000	7165	7104	7100	7156	7316
2	7531	0000	0262	0532	0743	1075	1134	1075	0743	0532
3	0262	0000	7531	7316	7156	7100	7104	7165	0000	0000
4	0000	0000	0000	0000	0000	0000	0000	0000	0000	0000
5	0000	0000	0000	0000	0000	0000	0000	0000	0000	0000
6	0000	0000	0000	0000	0000	0000	0000	0000	0000	0000
7	0000	0000	0000	0000	0000	0000	0000	0000	0000	0000
8	0000	0000	0000	0000	0000	0000	0000	0000	0000	0000
9	0000	0000	0000	0000	0000	0000	0000	0000	0000	0000

Notes:

This represents the filter points for Z1 (Channel 1) the rest are time shifted to beam MCF0 to 315° Az, 70° dist.

	0	1	2	3	4	5	6	7	8	9
0	0000	0000	0000	0000	0000	0000	0000	0000	0000	0000
1	0000	0000	0000	0000	0000	0000	0000	0000	0000	0000
2	0000	0000	0000	0000	0000	0000	3175	7355	7406	7440
3	7473	7526	7560	7612	7642	7670	7714	7735	7766	7775
4	0002	0003	0002	7776	0000	0000	0000	0000	0000	0000
5	0000	0000	0000	0000	0000	0000	0000	0000	0000	0000
6	0000	0000	0000	0000	0000	0000	0000	0000	0000	0000
7	0000	0000	0000	0000	0000	0000	0000	0000	0000	0000
8	0000	0000	0000	0000	0000	0000	0000	0000	0000	0000
9										

This represents the filter points for Z1 (channel) the rest are time shifted to beam MCF1 to 315° Az, 70° dist.

MCF Aux. Processor
Parameters and Settings

U.K. Process: Used ☐ Not Used ☑

Output 0	Output 1	History Length

Truncator _____
Output Setting 0 _____
Output Setting 1 _____

MCF Power Process: Used ☐ Not Used ☑

r intervals	s samples

Truncator _____
Output Setting 1 _____
Output Setting 2 _____
Output Setting 3 _____
Output Setting 4 _____

Fisher Process: Used ☑ Not Used ☐

N1	N2	History Length
777	040	060

Normalization Constants

Data Truncator 1
Σ Truncator 9
Output Setting -15

Notes:

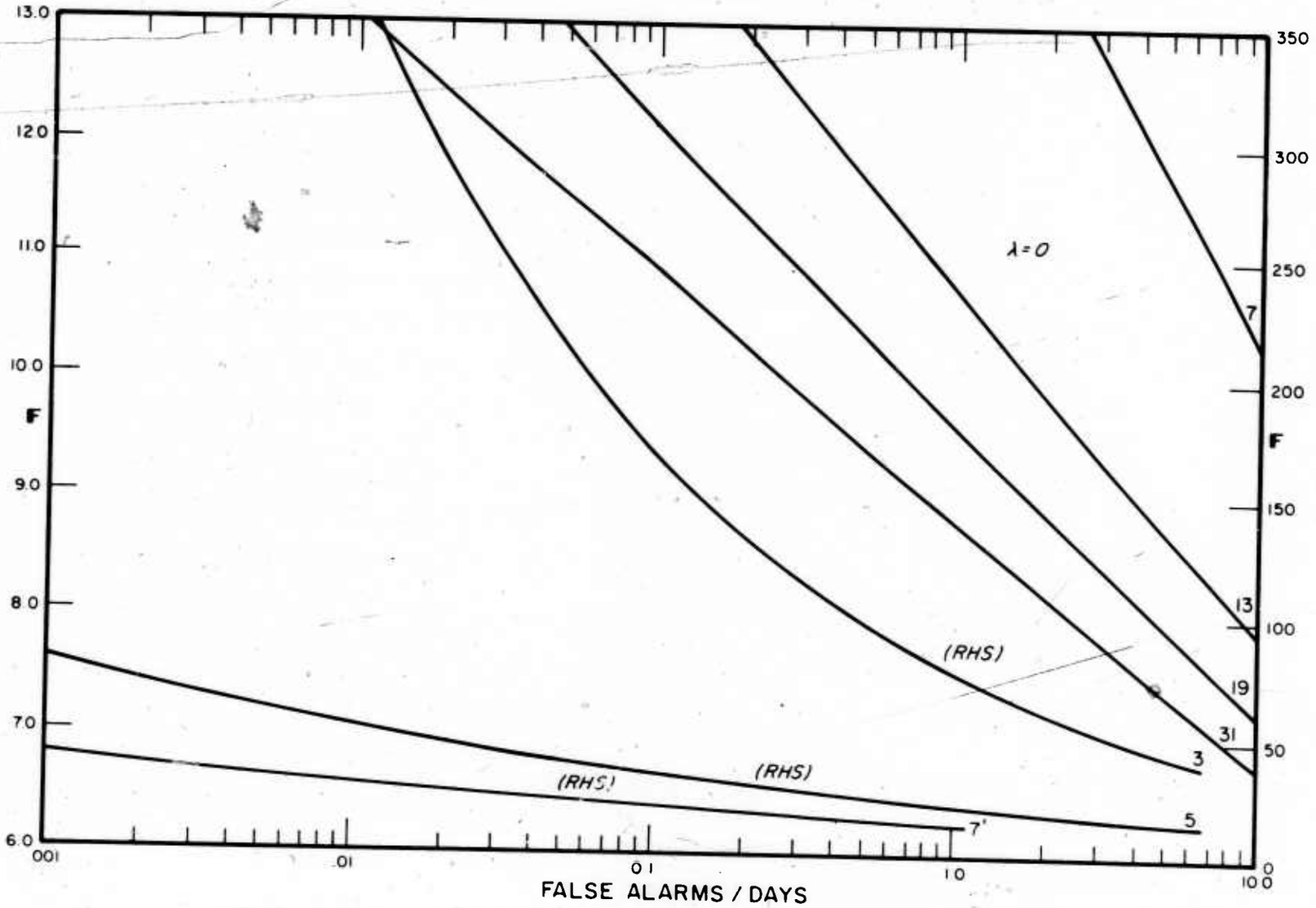

Figure 1. F values as a function of false alarm rate in false alarms per day for arrays with different numbers of elements.

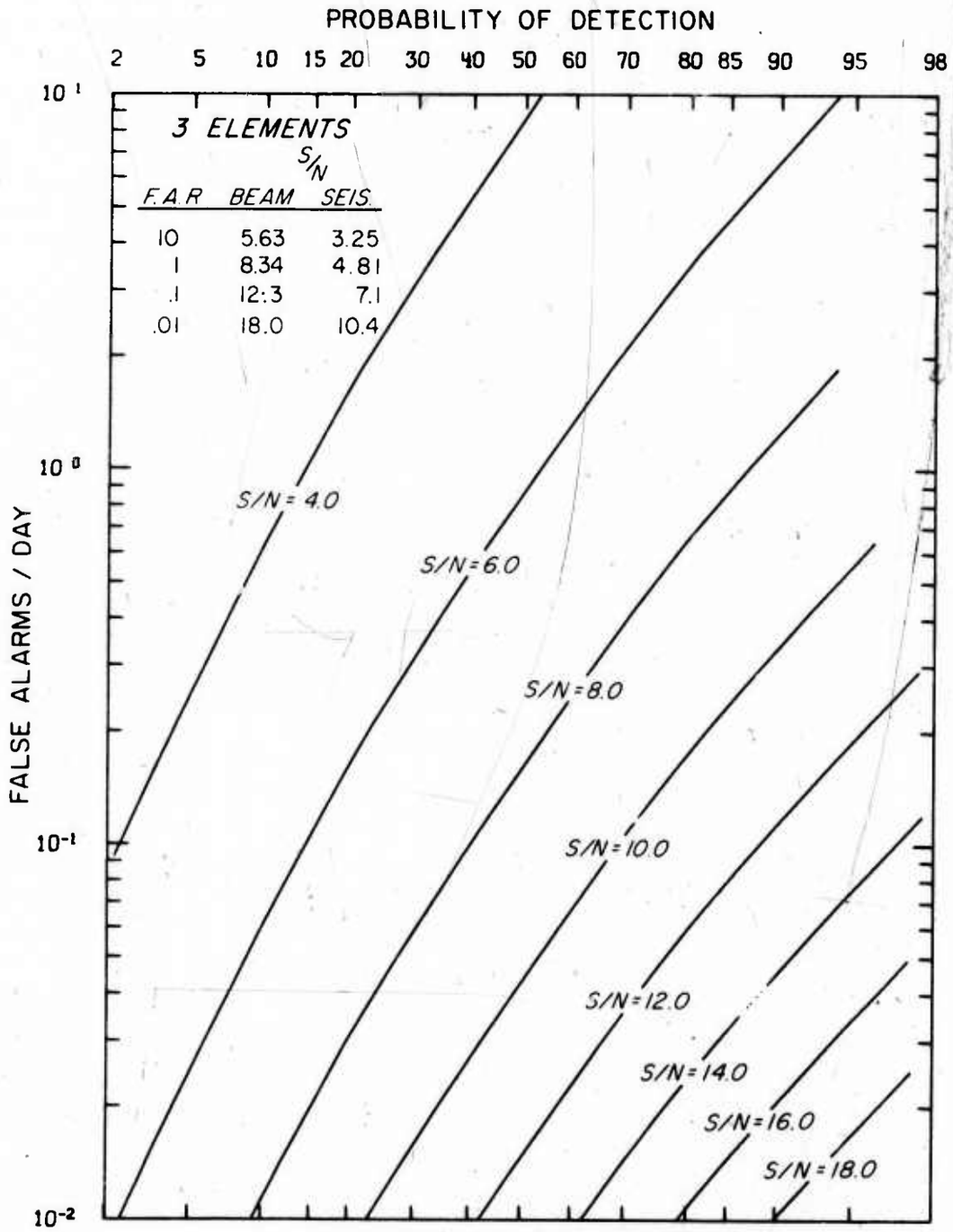

Figure 2. False alarms per day as a function of probability of detection for certain fixed signal to noise ratios on the array beam, and for 3 degrees of freedom in the numerator, 3 (N-1) in the denominator where N is the number of elements in the array. The figure is for an array of 3 elements.

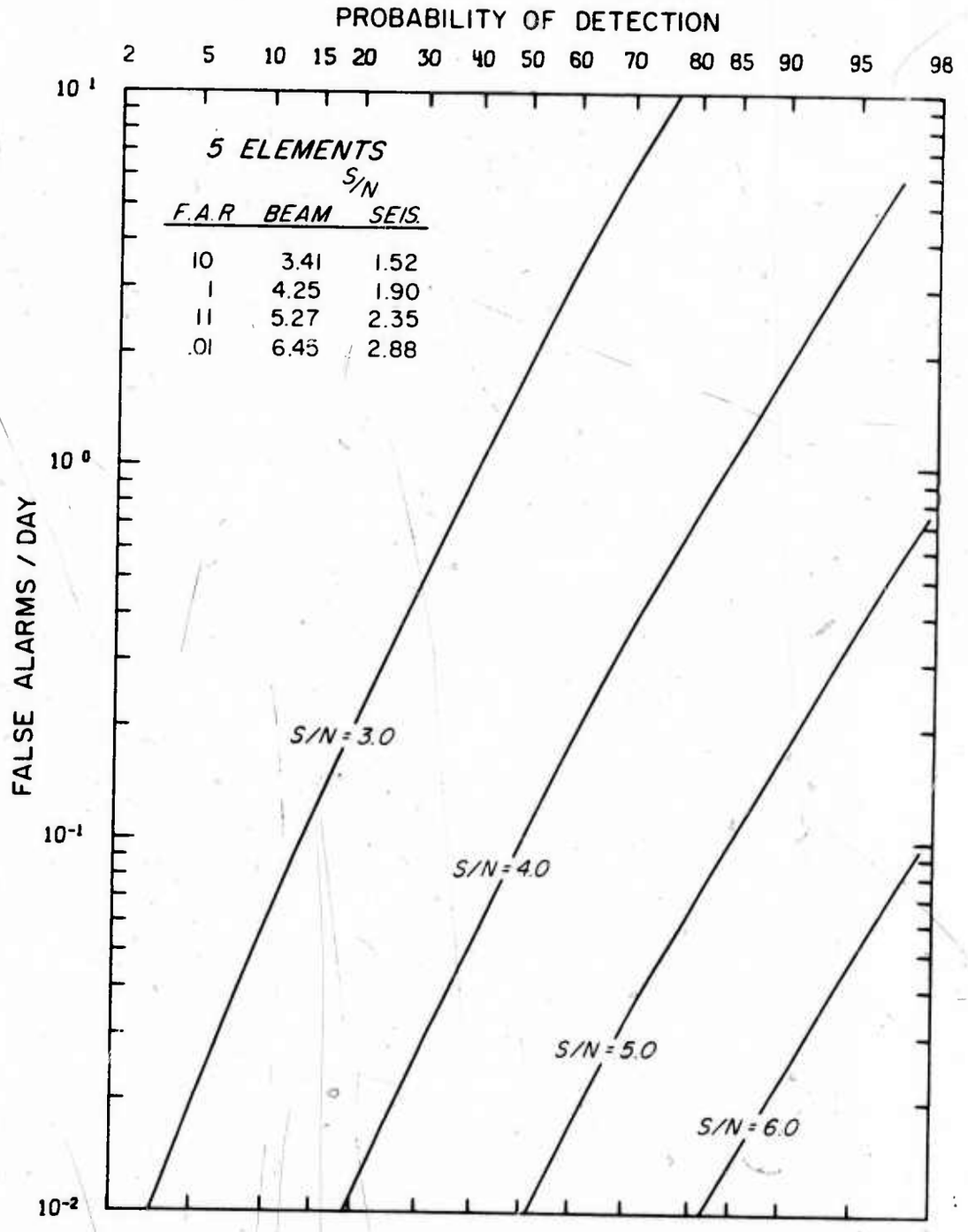

Figure 3. False alarms per day as a function of probability of detection for certain fixed signal to noise ratios on the array beam, and for 3 degrees of freedom in the numerator, 3 (N-1) in the denominator where N is the number of elements in the array. The figure is for an array of 5 elements.

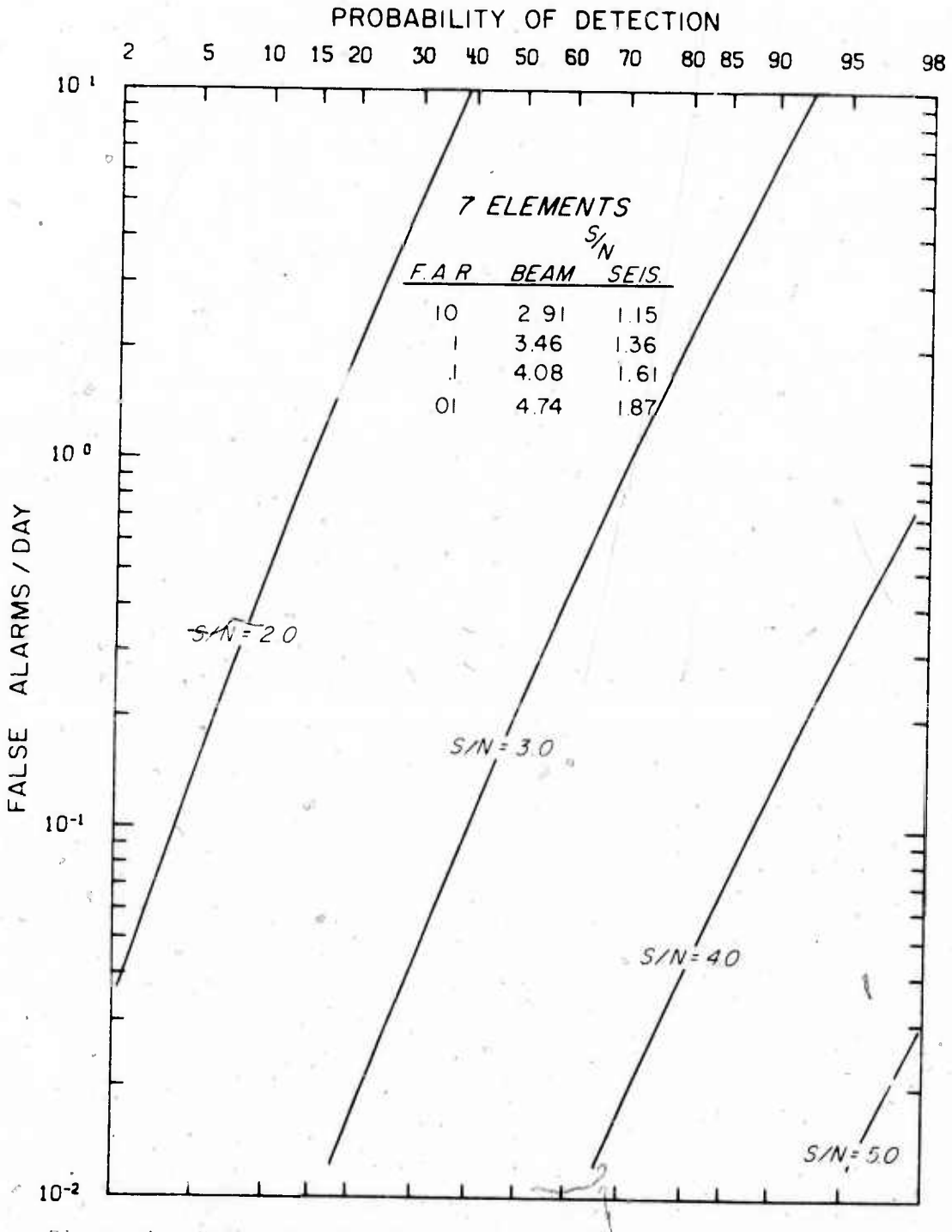

Figure 4. False alarms per day as a function of probability of detection for certain fixed signal to noise ratios on the array beam, and for 3 degrees of freedom in the numerator, 3 (N-1) in the denominator where N is the number of elements in the array. The figure is for an array of 7 elements.

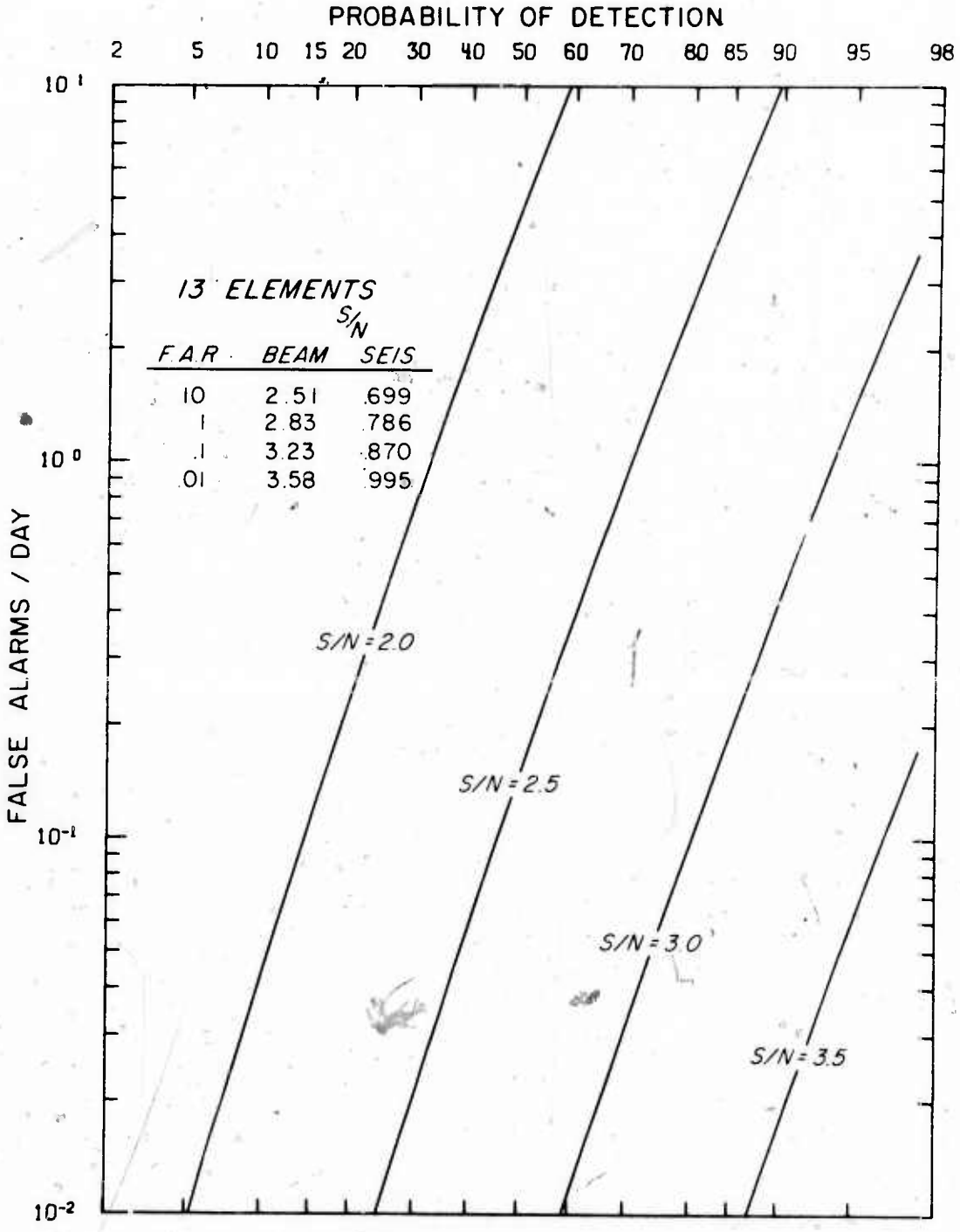

Figure 5. False alarms per day as a function of probability of detection for certain fixed signal to noise ratios on the array beam, and for 3 degrees of freedom in the numerator, 3 (N-1) in the denominator where N is the number of elements in the array. The figure is for an array of 13 elements.

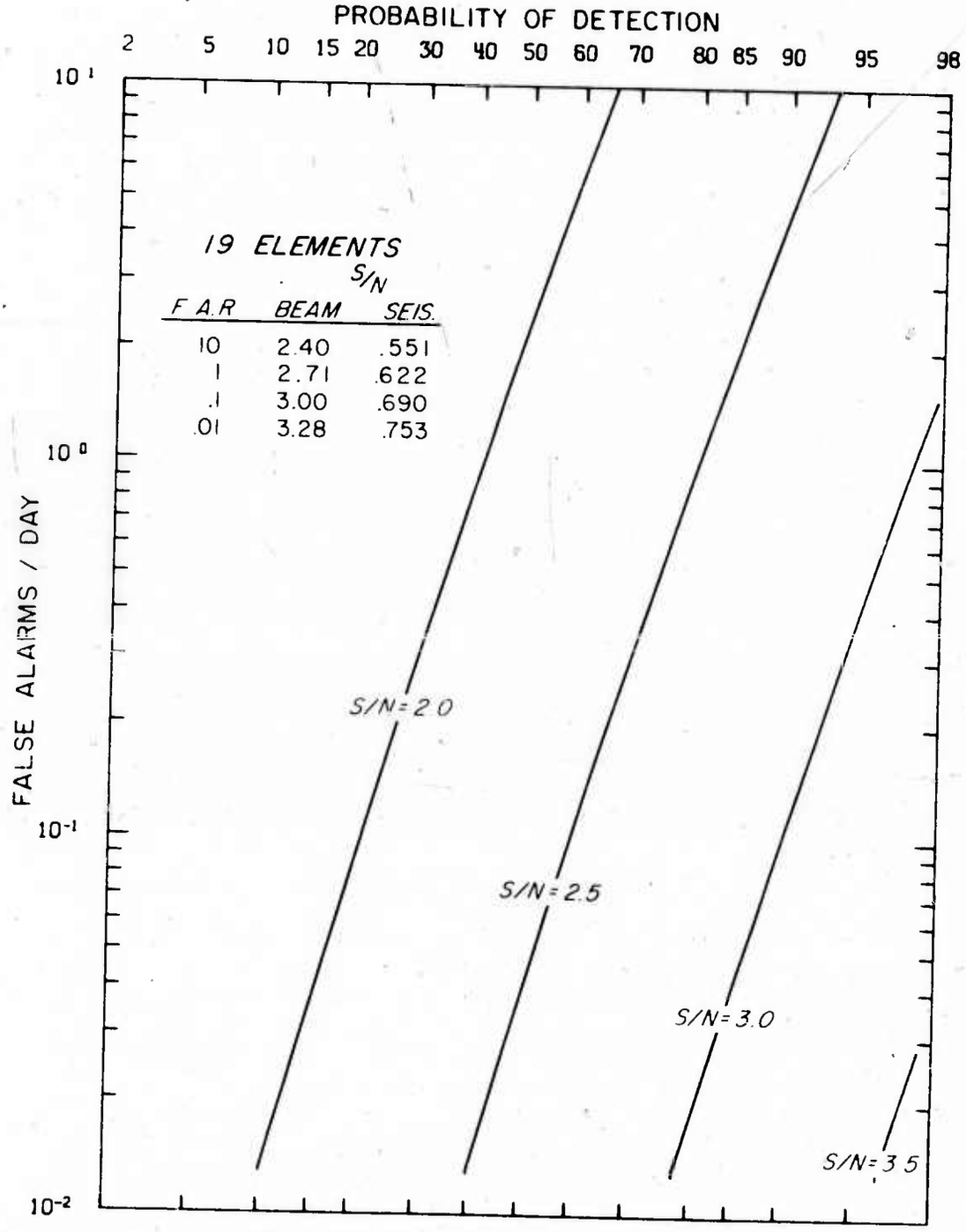

Figure 6. False alarms per day as a function of probability of detection for certain fixed signal to noise ratios on the array beam, and for 3 degrees of freedom in the numerator, 3 (N-1) in the denominator where N is the number of elements in the array. The figure is for an array of 19 elements.

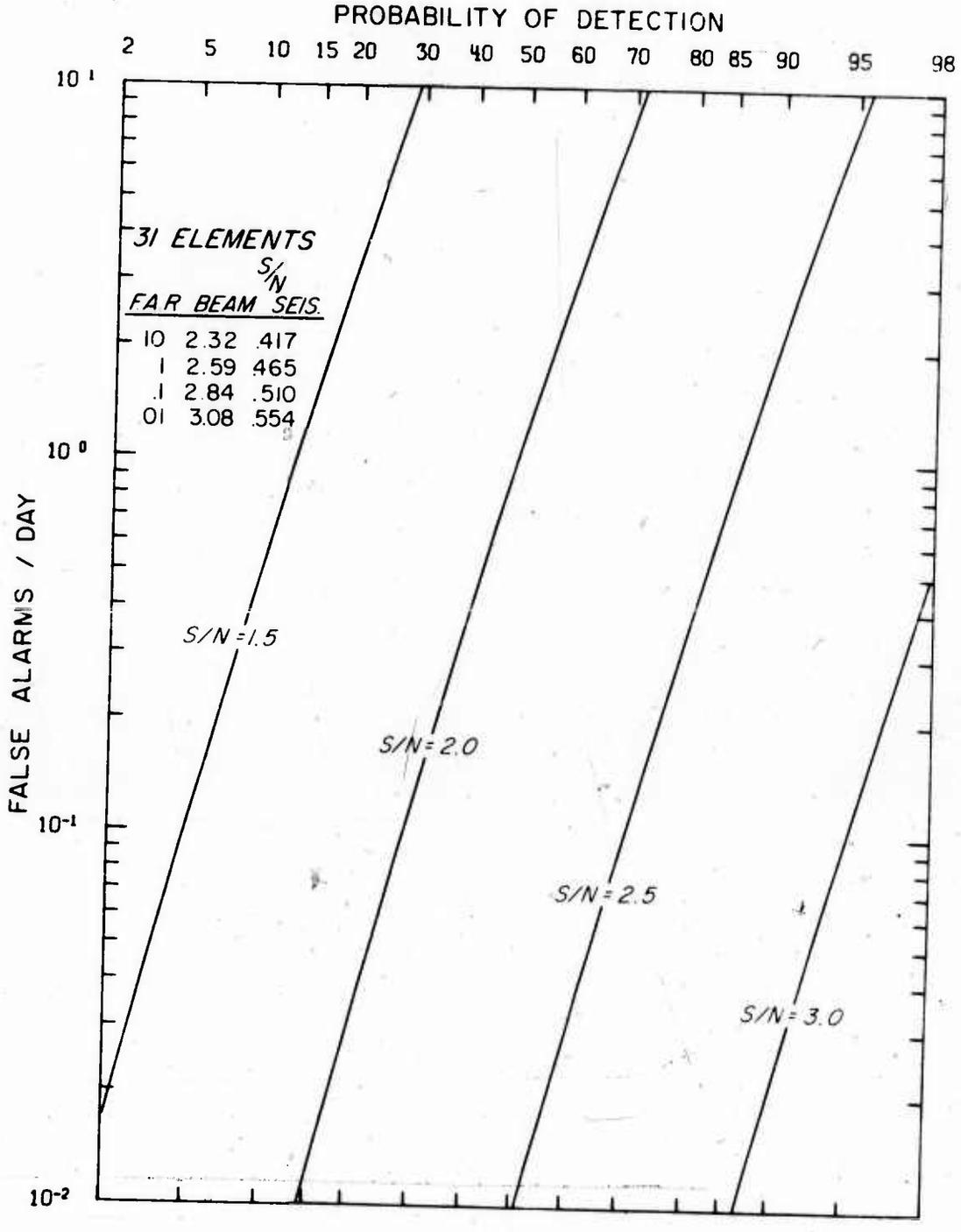

Figure 7. False alarms per day as a function of probability of detection for certain fixed signal to noise ratios on the array beam, and for 3° of freedom in the numerator 3 (N-1) in the denominator where N is the number of elements in the array. The figure is for an array of 31 elements.

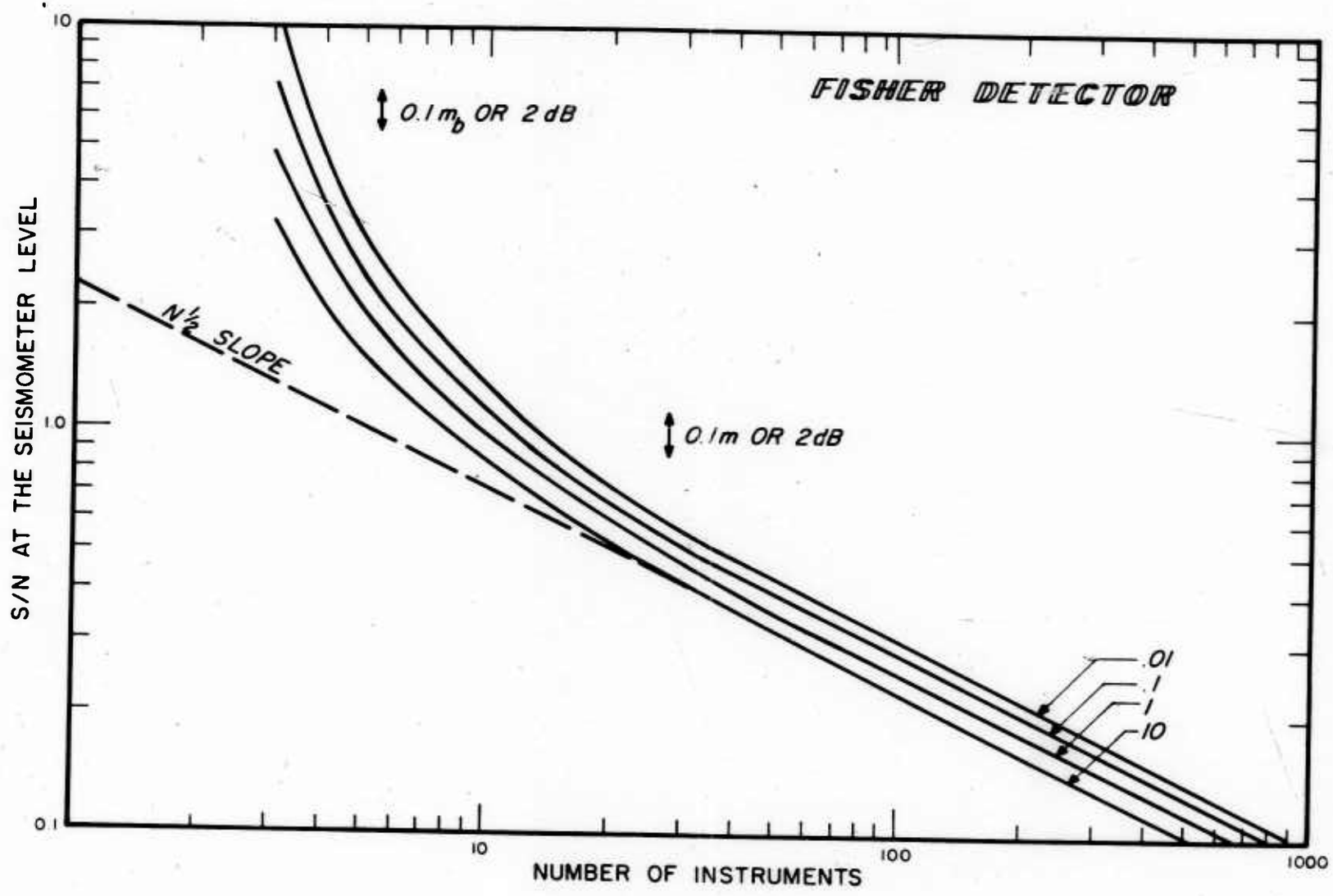

Figure 8. Signal to noise ratio required at the seismometer for 90% probability of detection as a function of the number of seismometers in the array, for different values of false alarms per day.

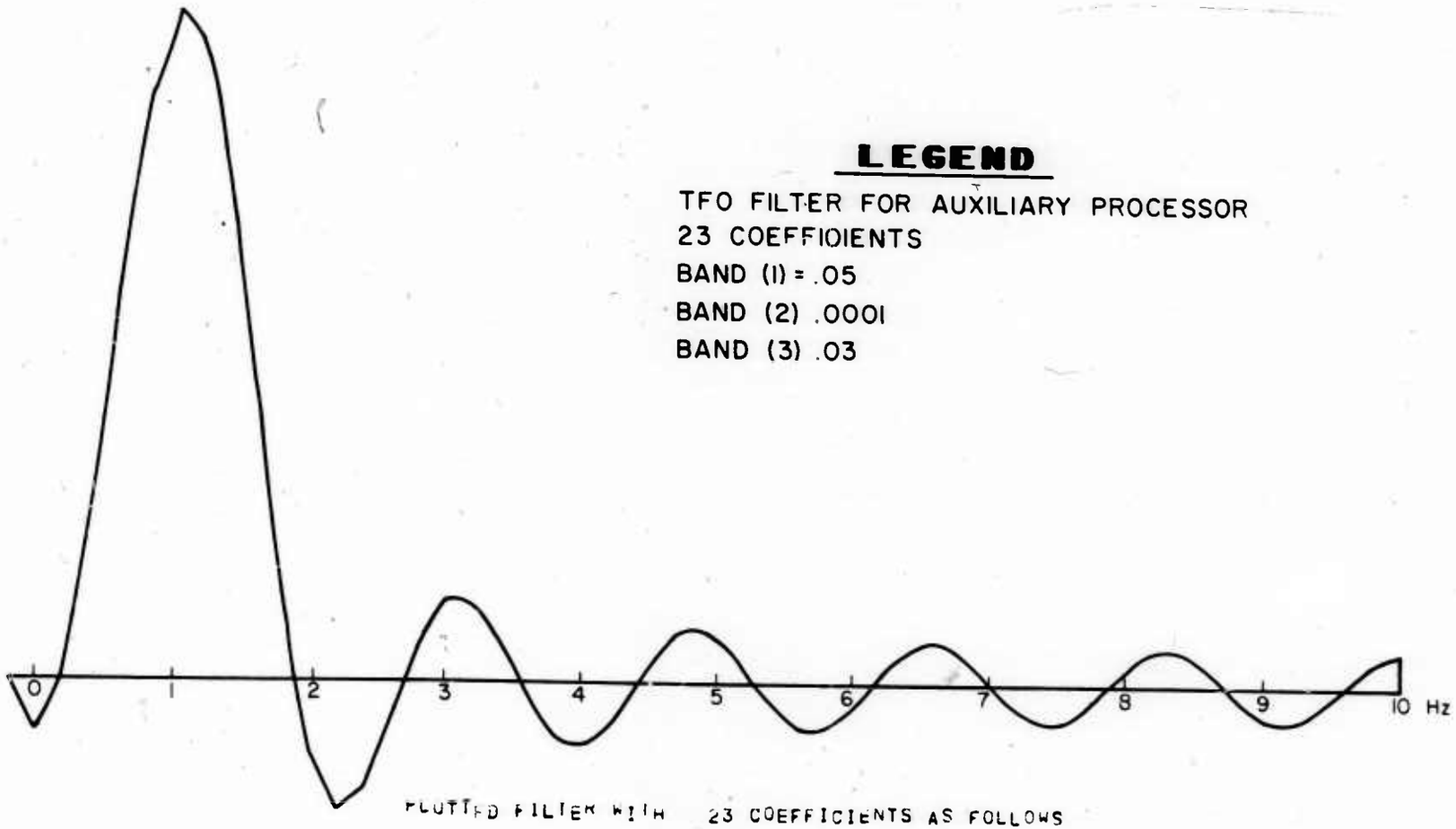

PLOTTED FILTER WITH 23 COEFFICIENTS AS FOLLOWS

I	COEF(I)	I	COEF(I)	I	COEF(I)	I	COEF(I)
1	-3.94945E-002	2	-4.44113E-002	3	-4.48471E-002	4	-4.02260E-002
5	-3.06106E-002	6	-1.67455E-002	7	.00000E 000	8	1.77913E-002
9	3.45600E-002	10	4.82040E-002	11	5.72728E-002	12	6.04000E-002
13	5.72728E-002	14	4.82040E-002	15	3.45600E-002	16	1.77913E-002
17	.00000E 000	18	-1.67455E-002	19	-3.06106E-002	20	-4.02260E-002
21	-4.48471E-002	22	-4.44113E-002	23	-3.94945E-002		

Figure 9. Bandpass prefilter for the Fisher detector.

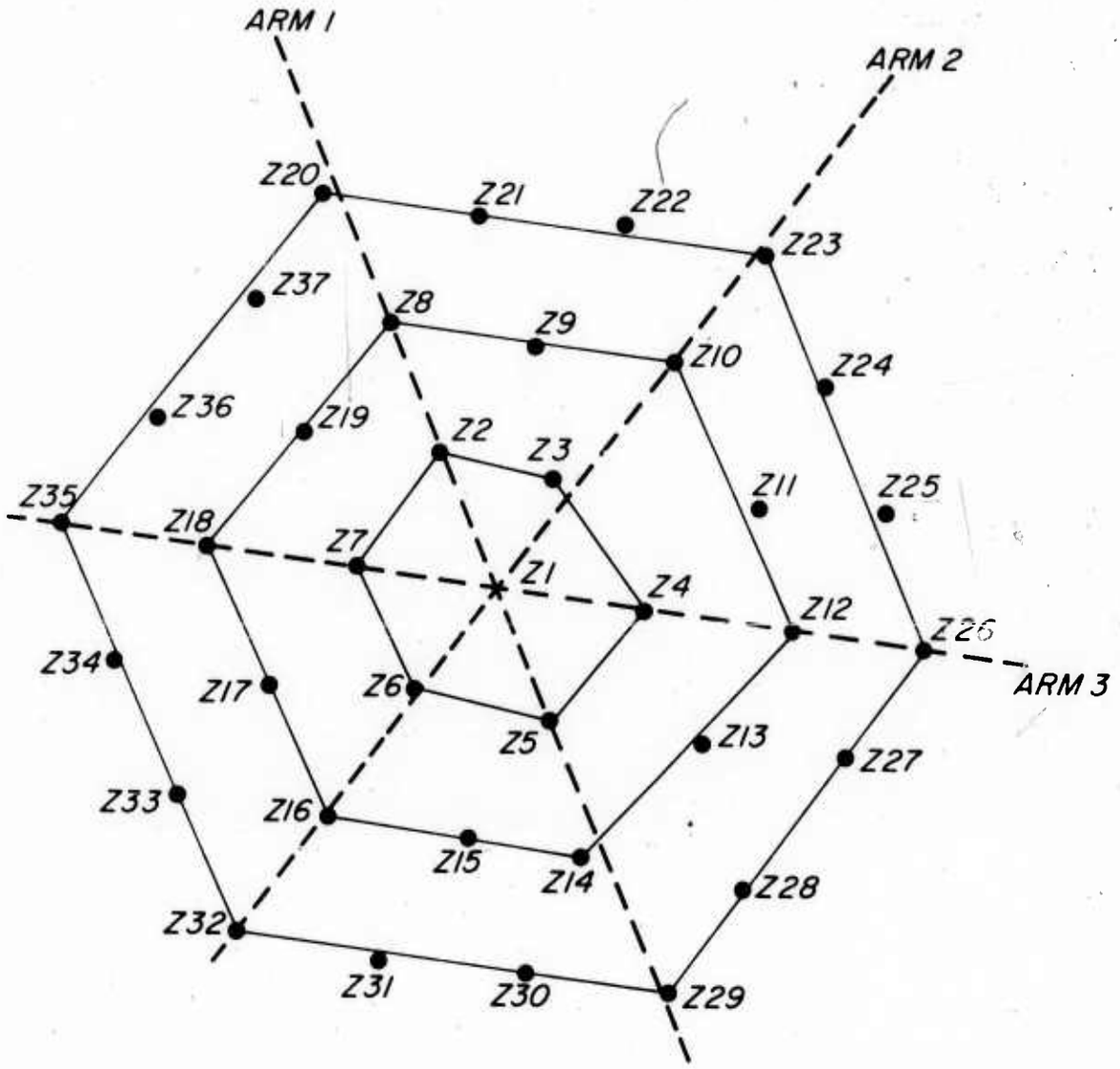

Figure 10. TFO 37-element array. Elements 3, 5, 7, 8, 12, and 16 not used in the Fisher detector.

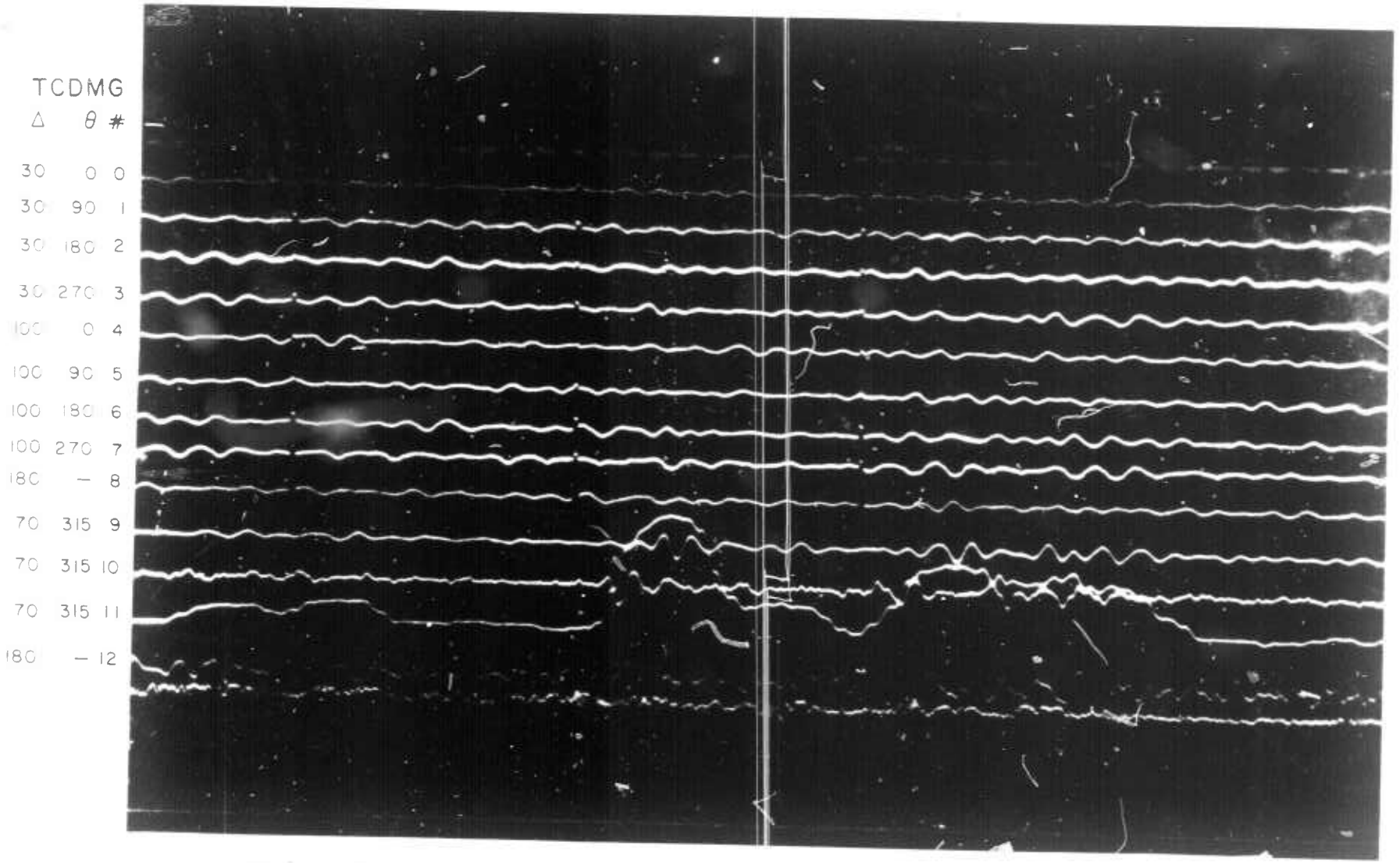

Figure 11. Detector response on 0732 April 25, 1970, trace 9 shows the Kuril beam through the filter shown in Figure 9. Trace 10 is through a broader filter, and trace 11 is the detector operating on trace 9.

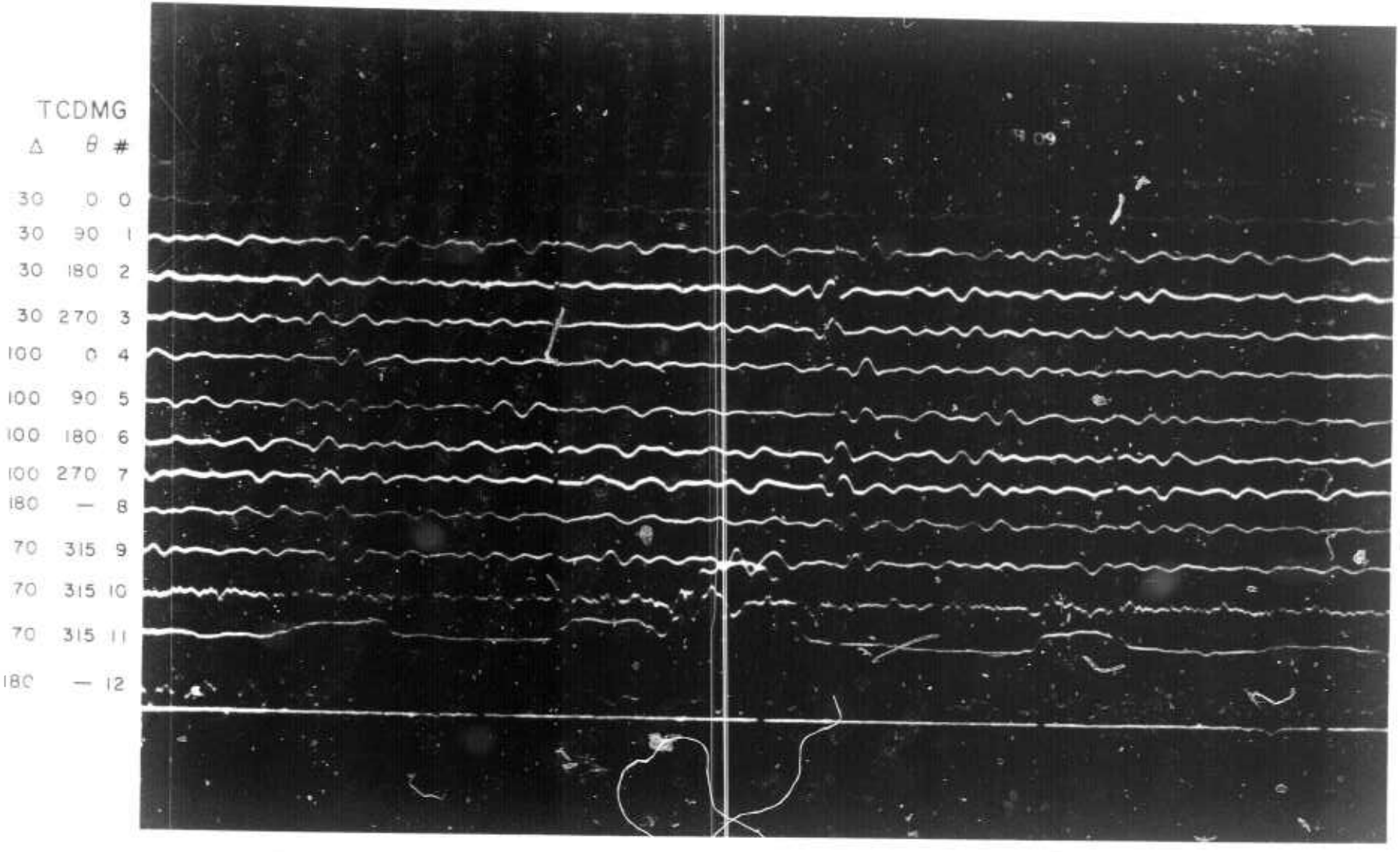

Figure 12. Detector response on 0111 April 9, 1970. Trace 9 shows the Kuril beam through the filter shown in Figure 9. Trace 10 is through a broader filter, and trace 11 is the detector operating on trace 9.

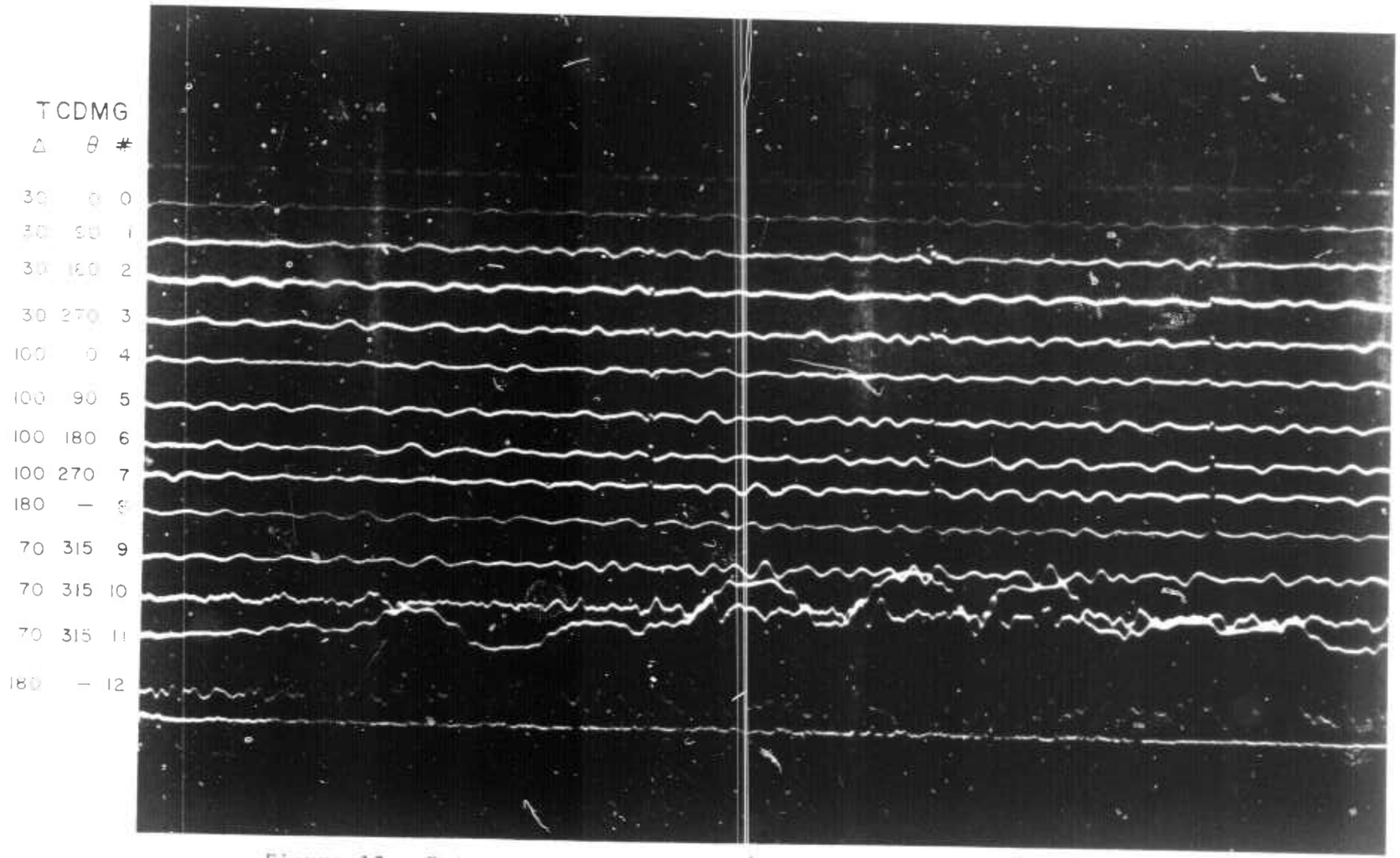

Figure 13. Detector response on 0644 April 25, 1970. Trace 9 shows the Kuril beam through the filter shown in Figure 9. Trace 10 is through a broader filter, and trace 11 is the detector operating on trace 9.

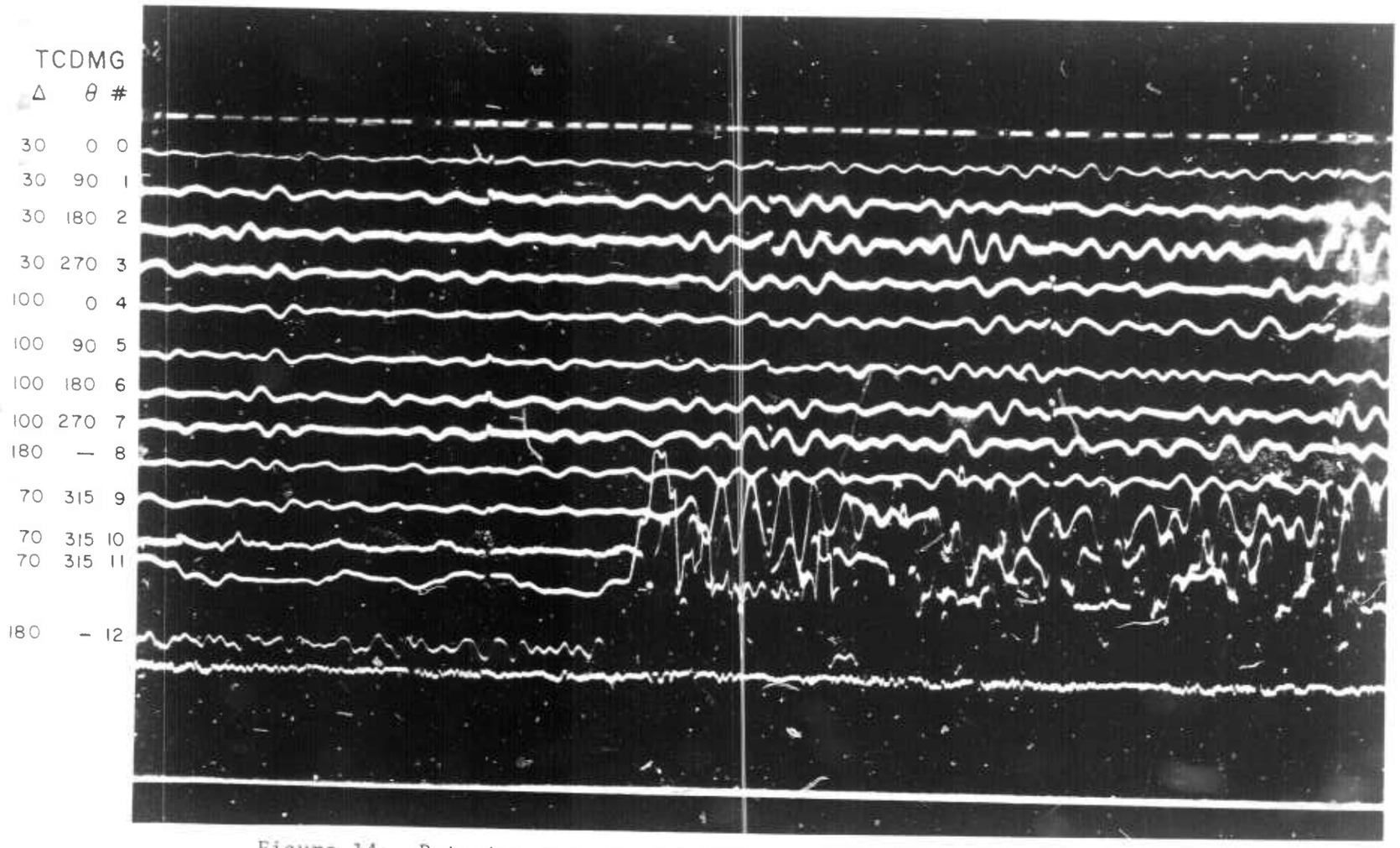

Figure 14. Detector response on 0052 April 8, 1970, showing breakdown of detector for large events. Trace 9 shows the Kuril beam through the filter shown in Figure 9. Trace 10 is through a broader filter, and trace 11 is the detector operating on trace 9.

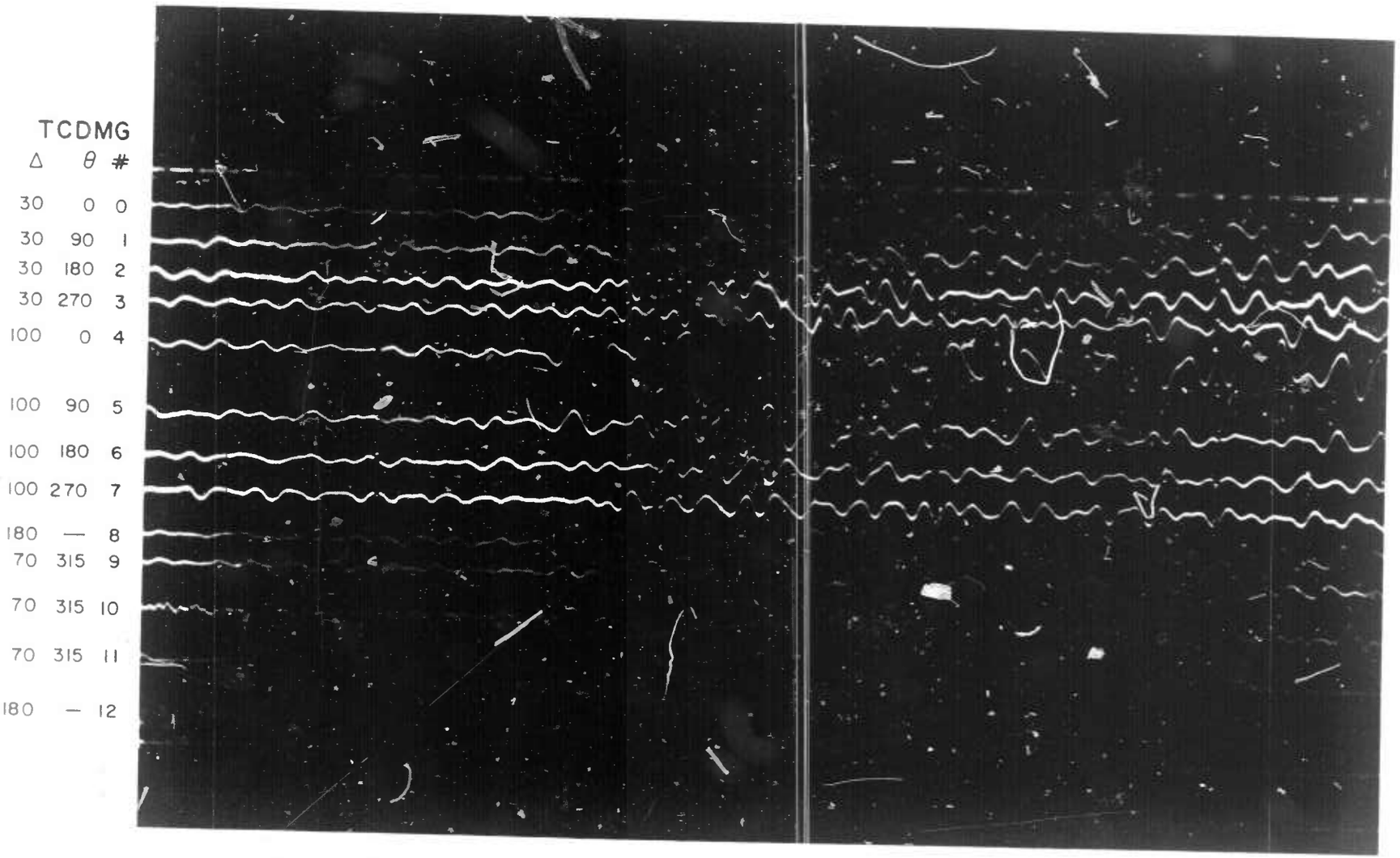

Figure 15. Detector response on 1343 April 19, 1970 showing detector response to off-beam event. Trace 9 shows the Kuril beam through the filter shown in Figure 9. Trace 10 is through a broader filter, and trace 11 is the detector operating on trace 9.

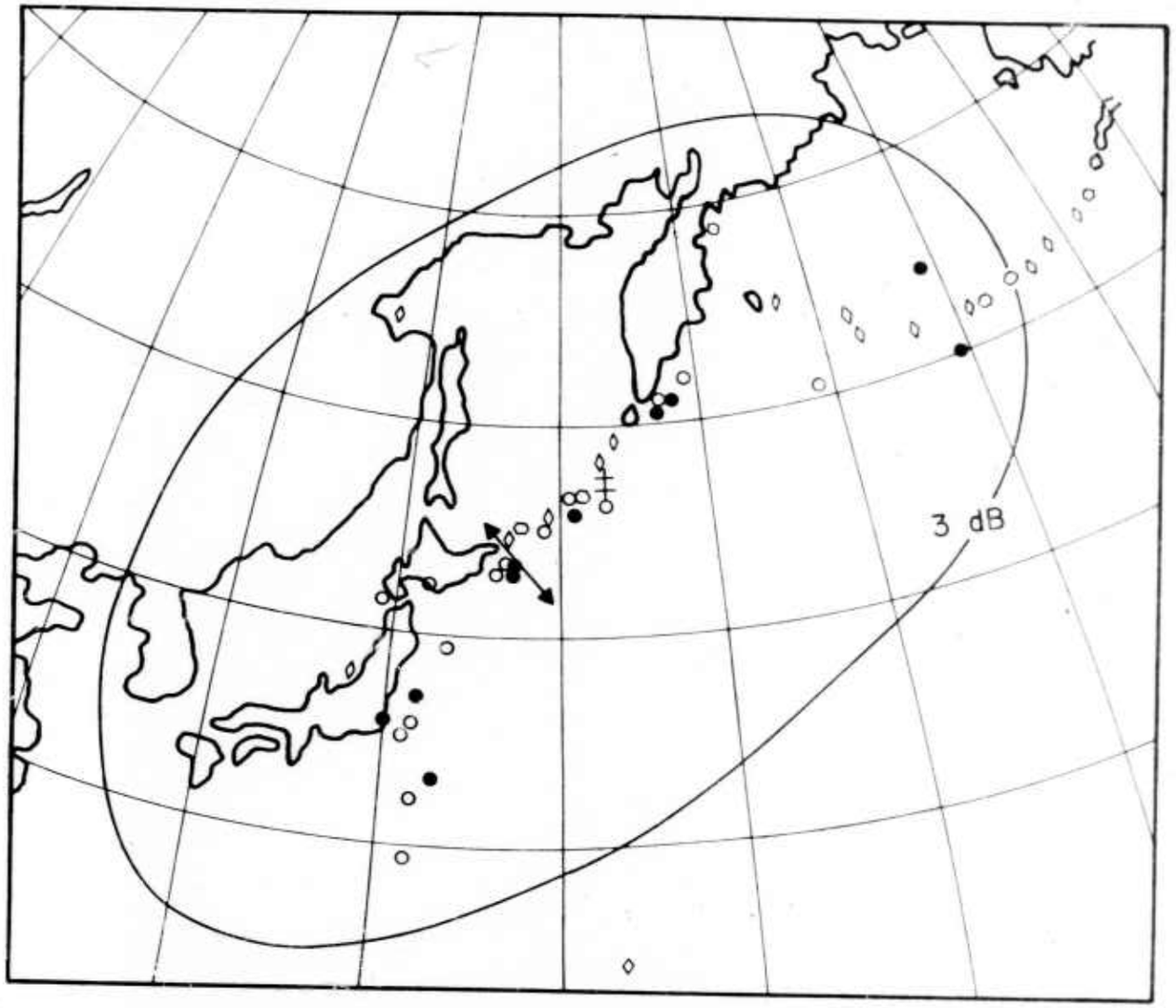

Figure 16. 3 dB contour of short-period TFO Kuril beam. Solid dots show 5.9 magnitude events with detector values greater than 7.0. Open dots have lesser values.

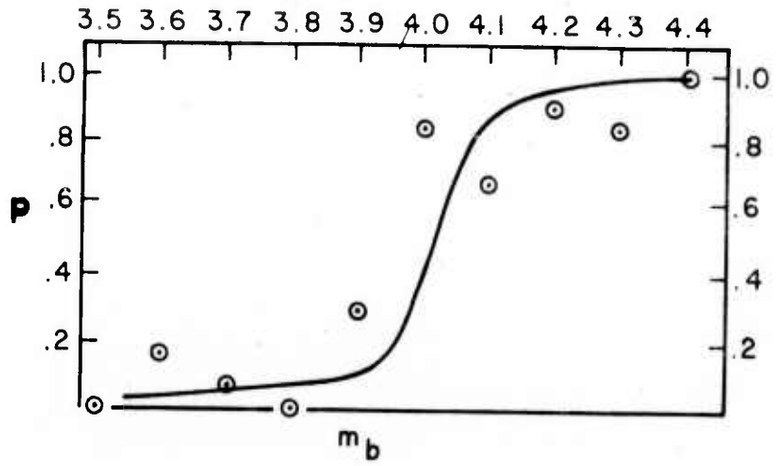

Figure 17. Probability of detection as a function of magnitude.

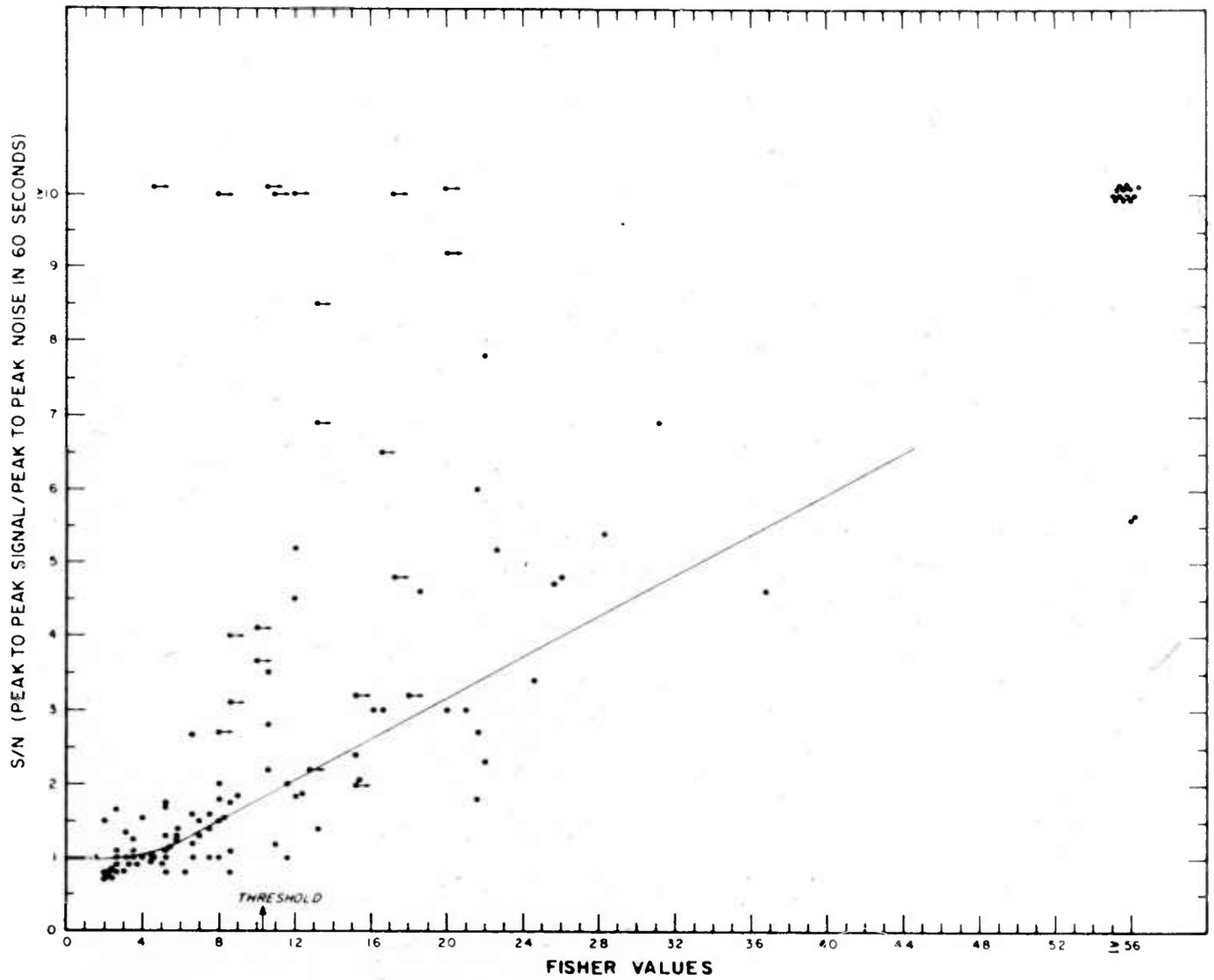

Figure 18. Signal to noise, peak to peak ratios as a function of the corresponding value on the Fisher detector. Arrow indicates F = 10.3 threshold.

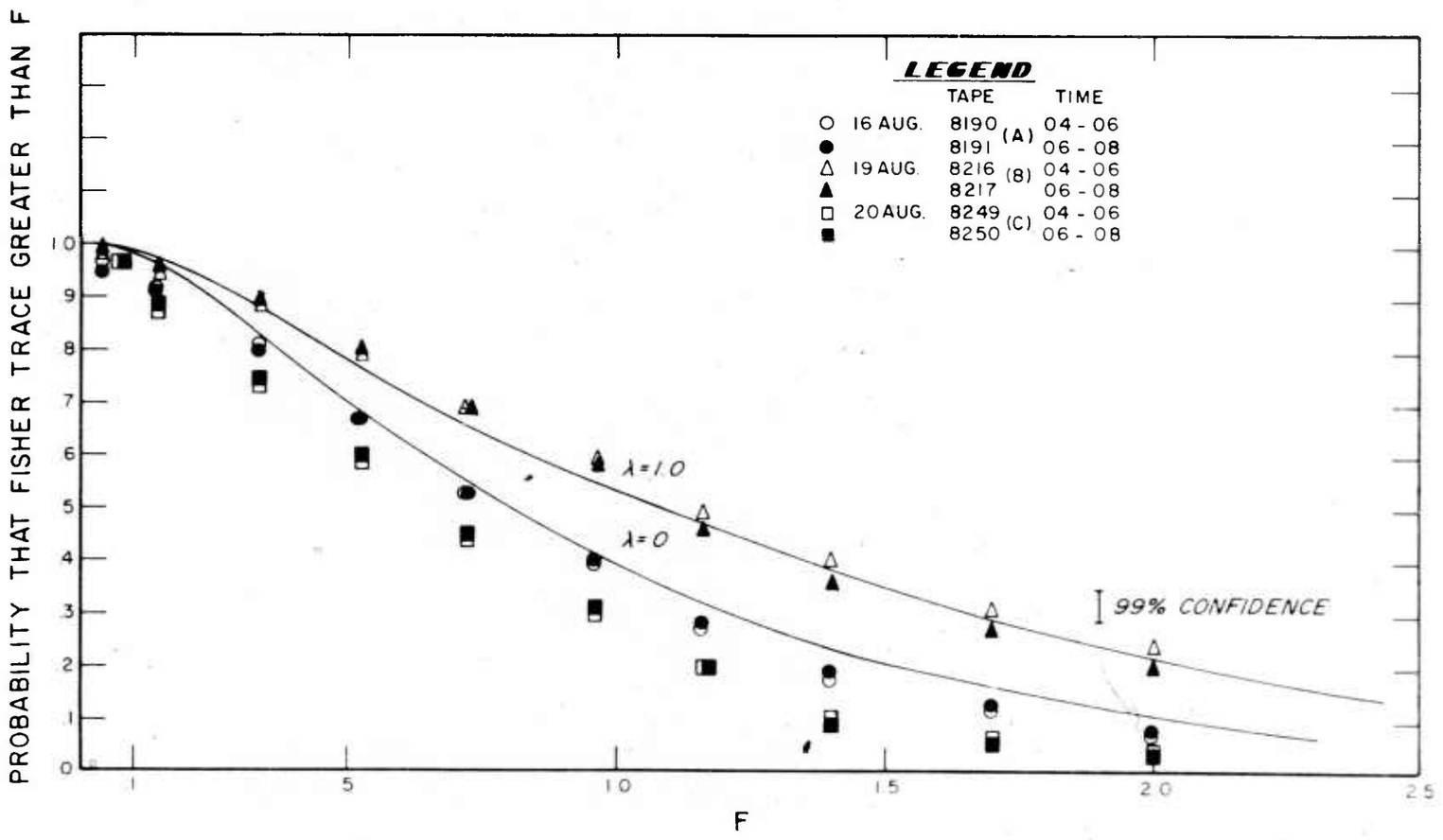

Figure 19. Probability that detector trace exceeds F as a function of F. Theoretical curves for λ = 0.0, and 1.0; experimental curves for three different days as noted, for each day histograms are given for successive two-hour periods.

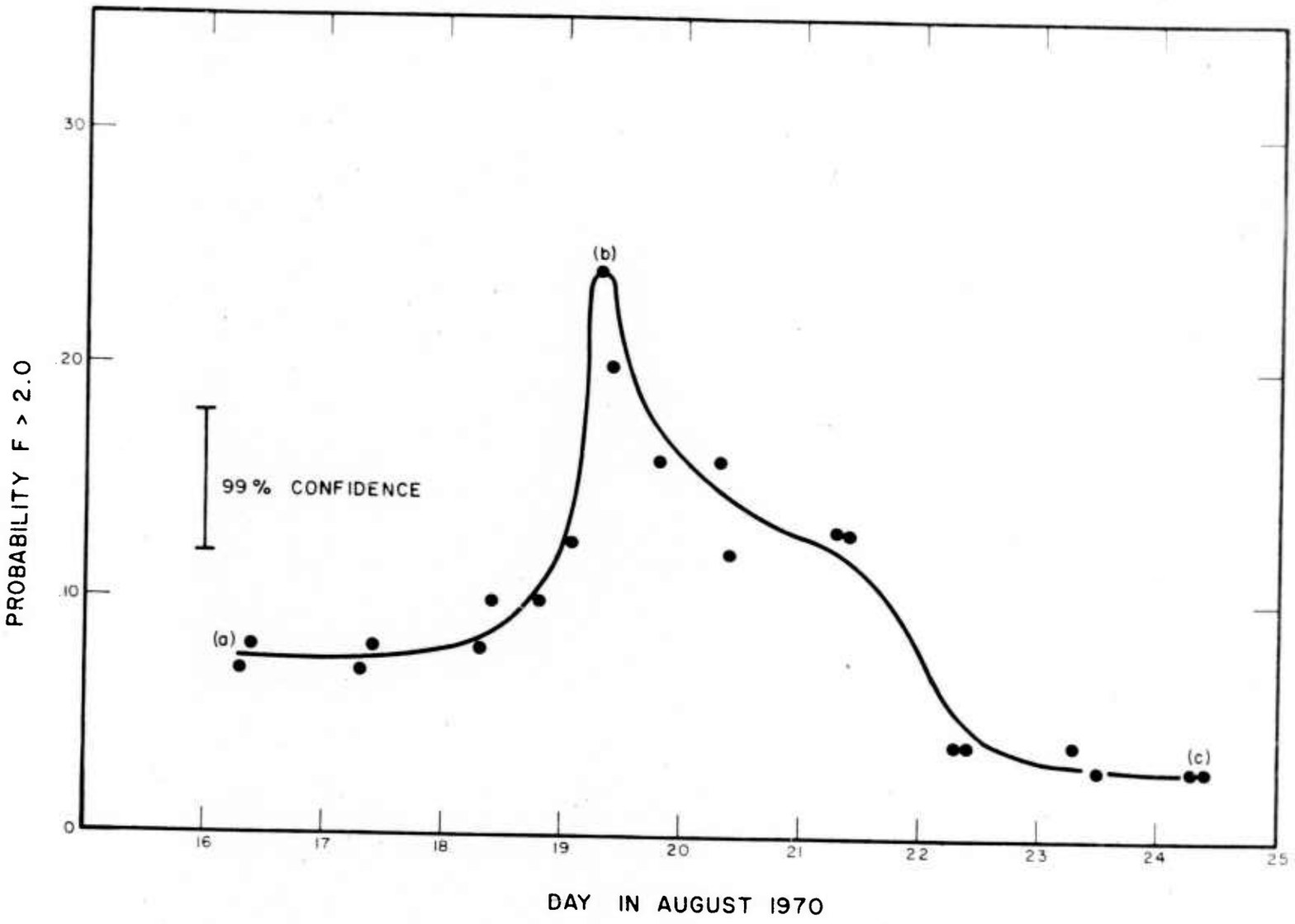

Figure 20. Probability that F > 2.0 on the Kuril beam as a function of time for the period August, 1970.

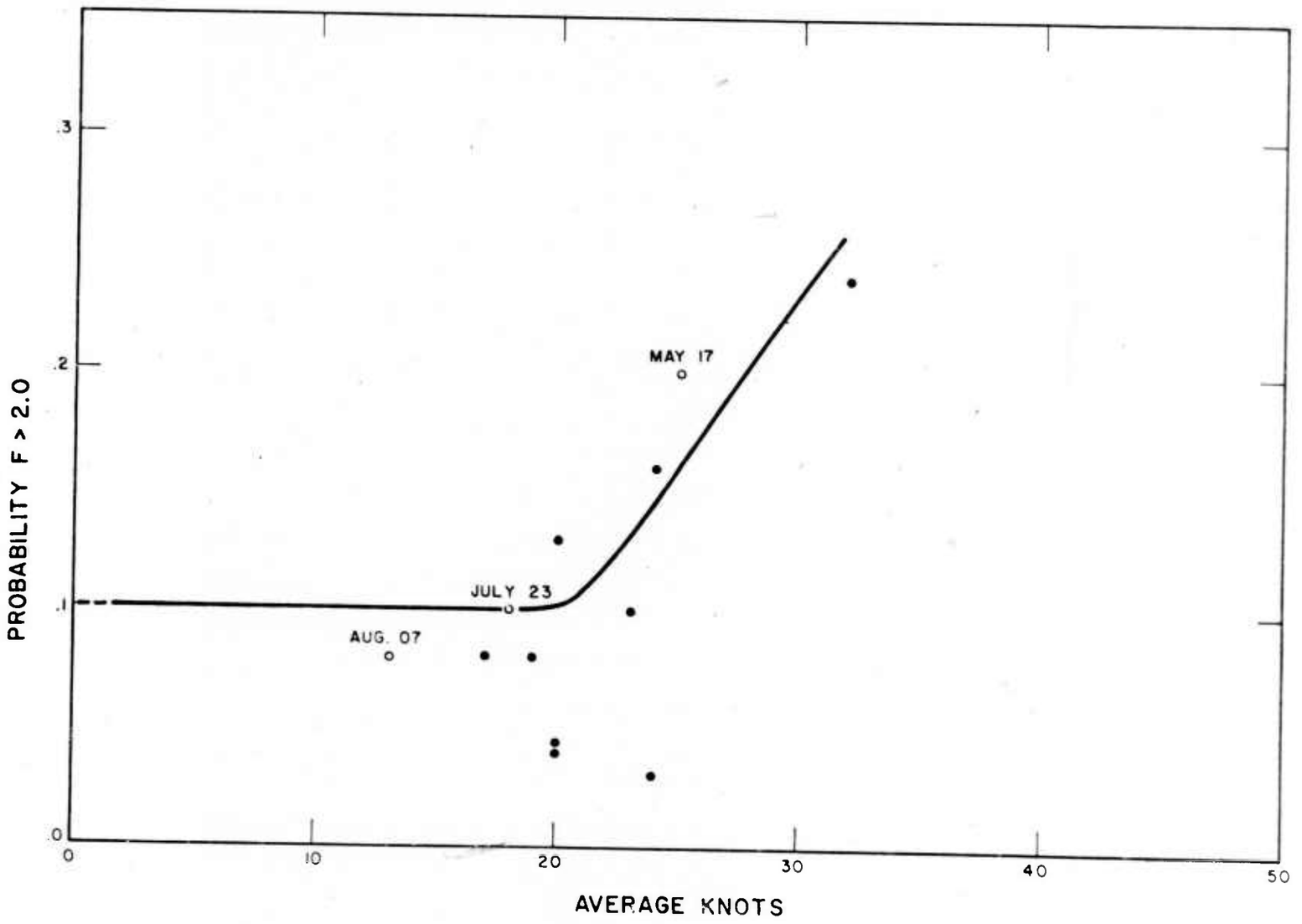

Figure 21. Probability that $\bar{F} \geq 2.0$ as a function of the average of the six highest velocity flags from United States weather maps inside the 3 db IFO contour. Letters indicate points for which maps are presented in Figure 22. Solid points are from August 16 through 24. Other points as indicated.

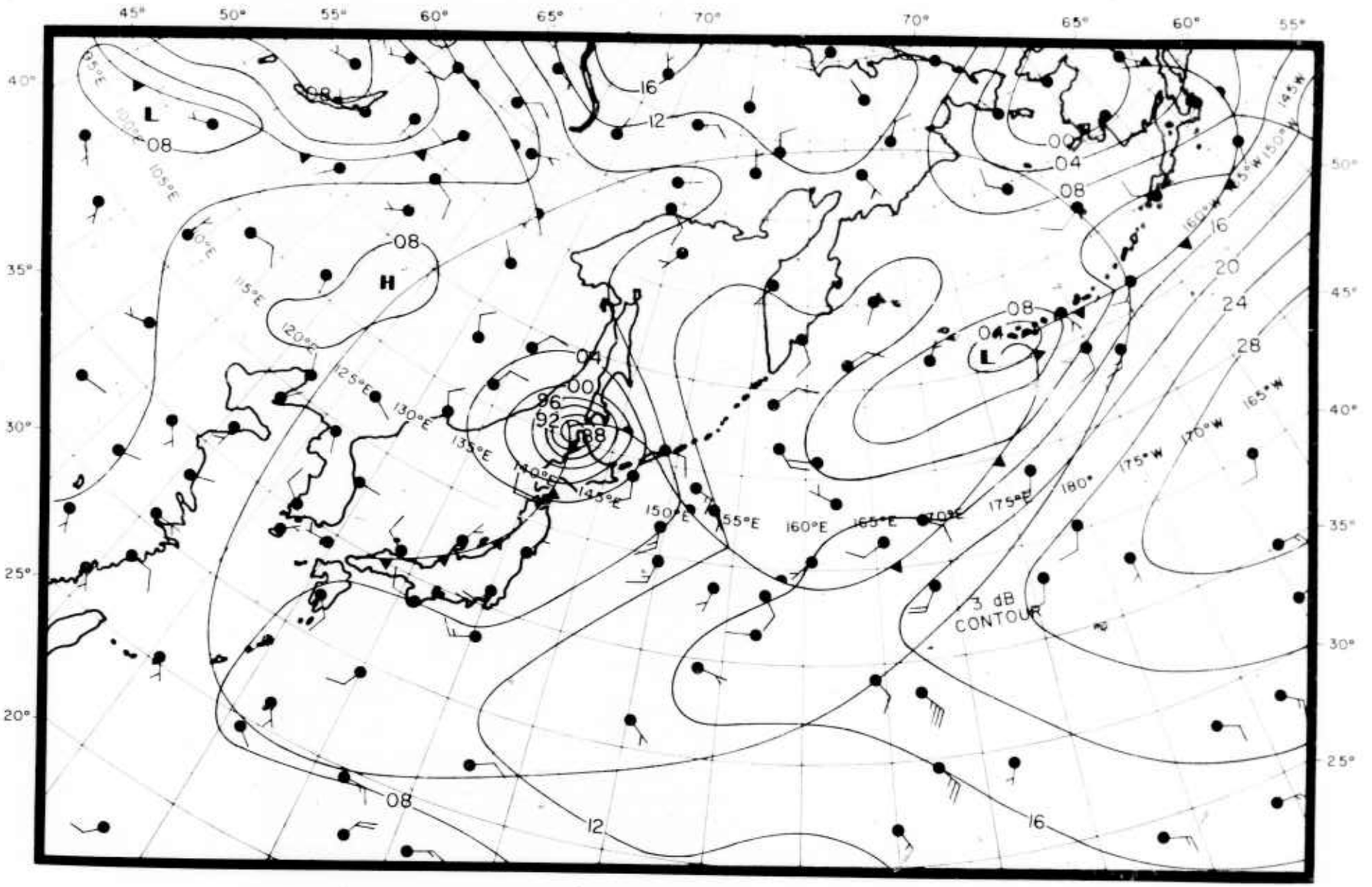

Figure 22a. United States Weather Bureau map for the points indicated by letters in Figures 19 and 20, August 16, 1970.

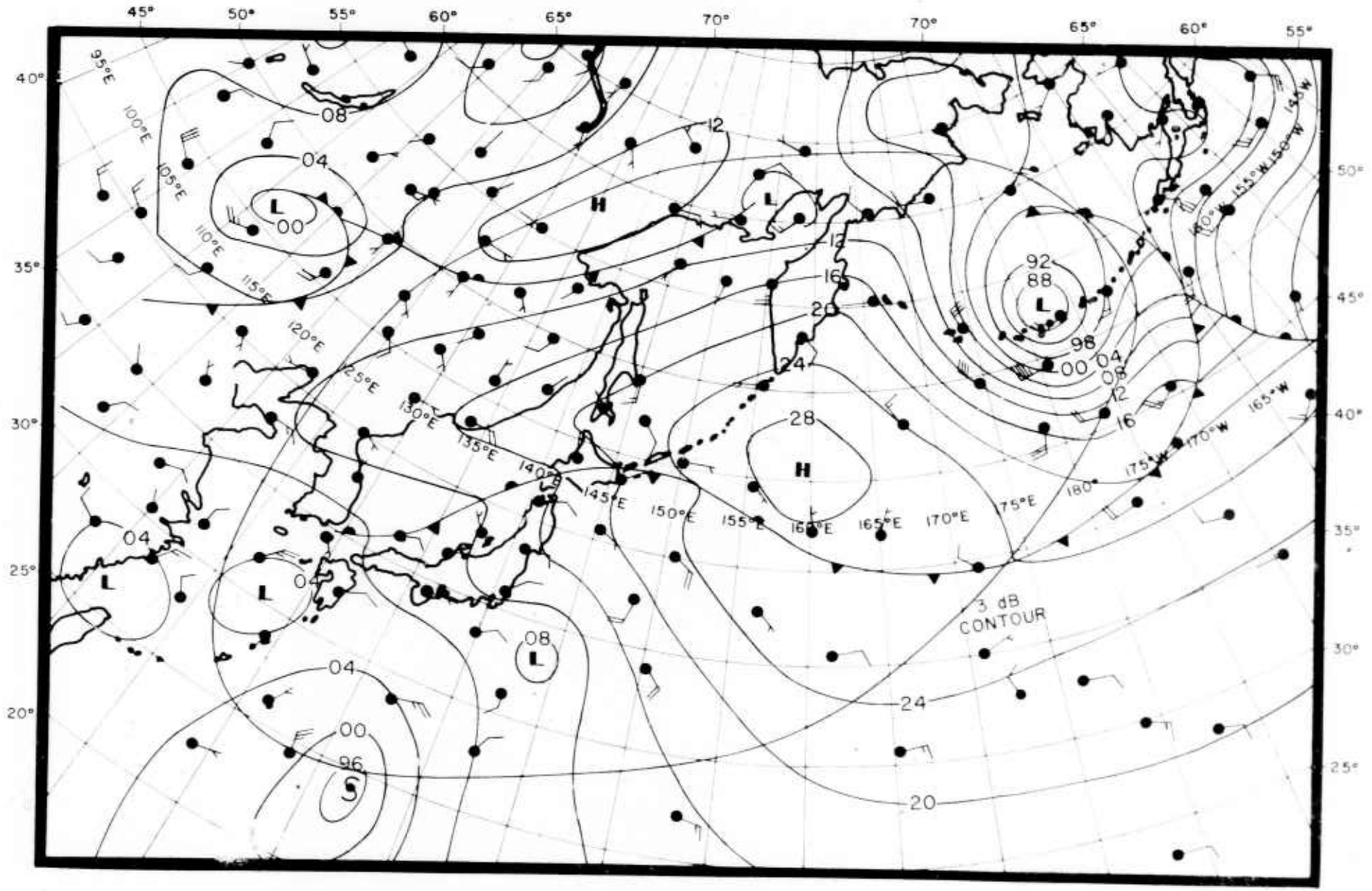

Figure 22b. United States Weather Bureau map for the points indicated by letters in Figures 19 and 20, August 19, 1970.

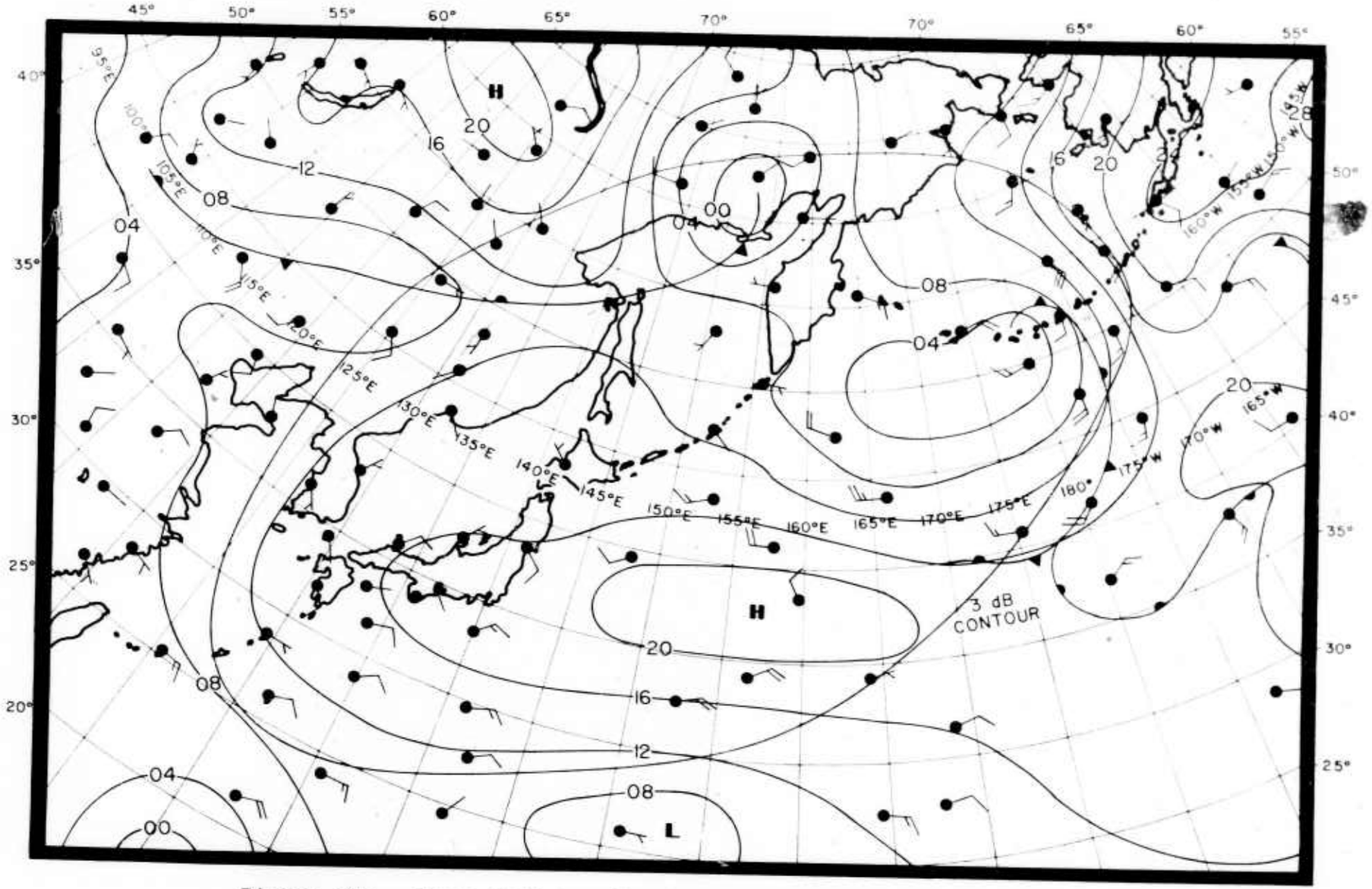

Figure 22c. United States Weather Bureau map for the points indicated by letters in Figures 19 and 20, August 24, 1970.

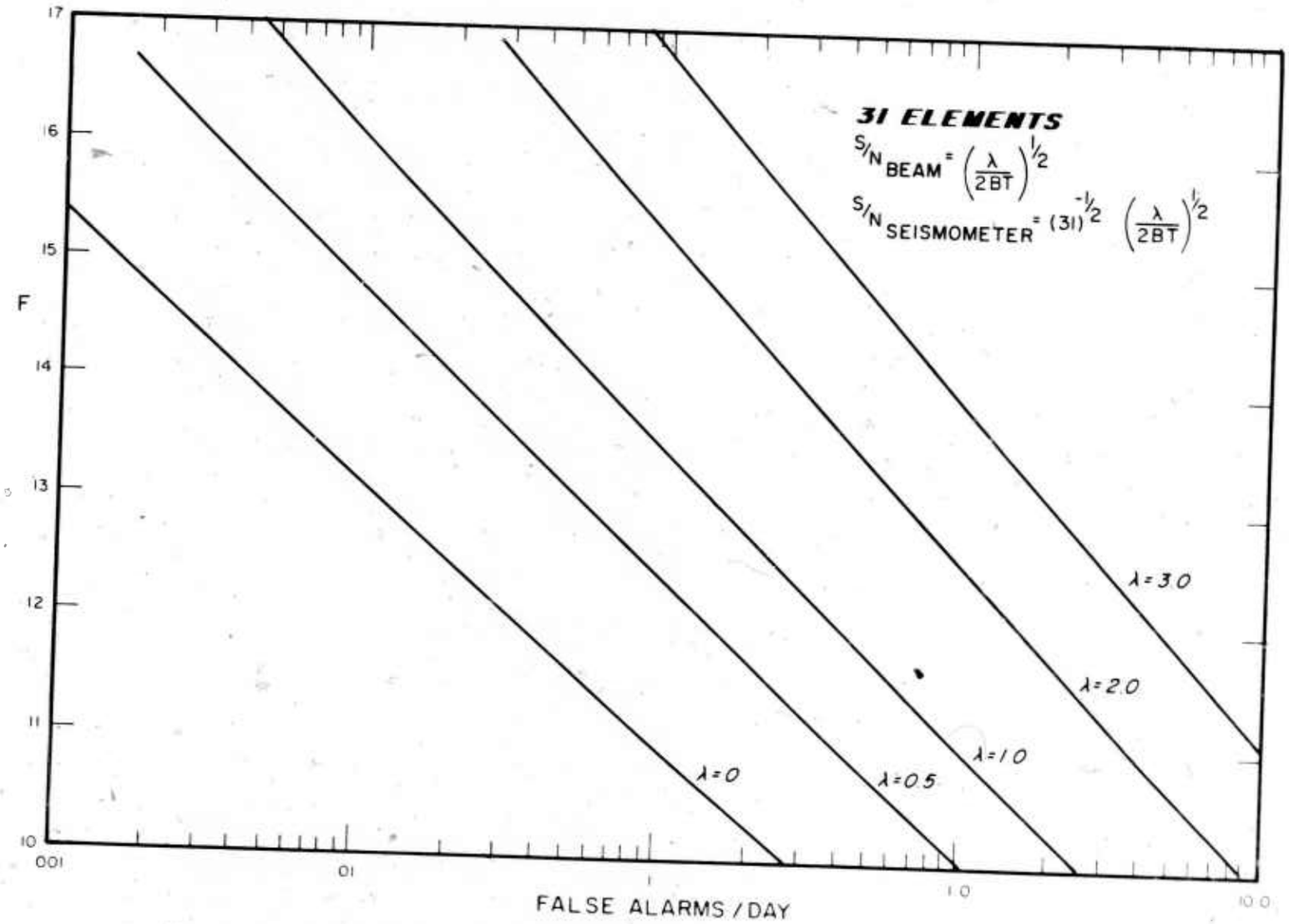

Figure 23. F values as a function of false alarm rate for a series of noncentrality parameters, for a 31-element array, 4° and 120° of freedom.

Unclassified

Security Classification

DOCUMENT CONTROL DATA - R&D

(Security classification of title, body of abstract and indexing annotation must be entered when the overall report is classified)

1 ORIGINATING ACTIVITY (Corporate author)
TELEDYNE GEOTECH
ALEXANDRIA, VIRGINIA

2a REPORT SECURITY CLASSIFICATION
Unclassified

2b GROUP

3 REPORT TITLE
AN AUTOMATIC EVENT DETECTOR AT TFO

4 DESCRIPTIVE NOTES (Type of report and inclusive dates)
Scientific

5 AUTHOR(S) (Last name, first name, initial)
Blandford, R.R.

6 REPORT DATE
18 November 1970

7a TOTAL NO. OF PAGES
68

7b NO. OF REFS
14

8a CONTRACT OR GRANT NO.
F33657-70-C-0941

b PROJECT NO
VELA T/0706

c
ARPA Order No. 624

d ARPA Program Code No. 9F10

9a ORIGINATOR'S REPORT NUMBER(S)
263

9b OTHER REPORT NO(S) (Any other numbers that may be assigned this report)

10 AVAILABILITY/LIMITATION NOTICES
This document is subject to special export controls and each transmittal to foreign governments or foreign nationals may be made only with prior approval of Chief, AFTAC.

11 SUPPLEMENTARY NOTES

12 SPONSORING MILITARY ACTIVITY
ADVANCED RESEARCH PROJECTS AGENCY
NUCLEAR MONITORING RESEARCH OFFICE
WASHINGTON, D. C.

13 ABSTRACT

The on-line operation of a Fisher detector has been evaluated at the Tonto Forest Observatory short-period seismic array. Using 31 seismometers and one fixed threshold, the 90 percent incremental detection threshold on the Kuril Islands beam, centered at $\Delta=70°$, is $m_b = 4.15 \pm .05$; with an experimentally determined false alarm rate of 0.17 per day. This compares favorably with the capabilities of a human operator. Storms in the Kurils significantly affect the distribution of amplitudes of the Fisher detection trace; and we estimate that most of the false alarms observed at the operating threshold can be traced to the statistical bias introduced by this storm generated energy. If the threshold were adjusted to maintain a constant false alarm rate, the maximum effect on the threshold magnitude would be 0.05 m_b.

14 KEY WORDS

Detection
Automatic Detection
Seismology,
Arrays
Seismic Arrays

Unclassified

Security Classification